European Journal of Medicinal Chemistry 105 (2015) 156–170

Contents lists available at ScienceDirect

European Journal of Medicinal Chemistry

journal homepage: http://www.elsevier.com/locate/ejmech

Research paper

Synthesis of novel flavone hydrazones: *In-vitro* evaluation of α-glucosidase inhibition, QSAR analysis and docking studies

Syahrul Imran [a, b], Muhammad Taha [a, b, *], Nor Hadiani Ismail [a, b, **], Syed Muhammad Kashif [c], Fazal Rahim [d], Waqas Jamil [c], Maywan Hariono [e], Muhammad Yusuf [e], Habibah Wahab [e]

[a] Atta-ur-Rahman Institute for Natural Product Discovery, Universiti Teknologi MARA, Puncak Alam Campus, 42300, Selangor D.E., Malaysia
[b] Faculty of Applied Sciences, Universiti Teknologi MARA, Shah Alam, 40450, Selangor D.E., Malaysia
[c] Institute of Advance Research Studies in Chemical Sciences, University of Sindh, 76080, Jamshoro, Pakistan
[d] Department of Chemistry, Hazara University, 21300, Mansehra, Pakistan
[e] Pharmaceutical Design and Simulation Laboratory, School of Pharmaceutical Sciences, Universiti Sains Malaysia, 11800, Pulau Pinang, Malaysia

ARTICLE INFO

Article history:
Received 25 May 2015
Received in revised form
8 September 2015
Accepted 7 October 2015
Available online xxx

Keywords:
Flavone
Hydrazone
α-Glucosidase
2D-QSAR
Docking

ABSTRACT

Thirty derivatives of flavone hydrazone (**5**–**34**) had been synthesized through a five-step reaction and screened for their α-glucosidase inhibition activity. Chalcone **1** was synthesized through aldol condensation then subjected through oxidative cyclization, esterification, and condensation reaction to afford the final products. The result for baker's yeast α-glucosidase (EC 3.2.1.20) inhibition assay showed that all compounds are active with reference to the IC_{50} value of the acarbose (standard drug) except for compound **3**. Increase in activity observed for compounds **2** to **34** clearly highlights the importance of flavone, hydrazide and hydrazone linkage in suppressing the activity of α-glucosidase. Additional functional group on *N*-benzylidene moiety further enhances the activity significantly. Compound **5** (15.4 ± 0.22 μM), a 2,4,6-trihydroxy substituted compound, is the most active compound in the series. Other compounds which were found to be active are those having chlorine, fluorine, and nitro substituents. Compounds with methoxy, pyridine, and methyl substituents are weakly active. Further studies showed that they are not active in inhibiting histone deacetylase activity and do not possess any cytotoxic properties. QSAR model was being developed to further identify the structural requirements contributing to the activity. Using Discovery Studio (DS) 2.5, various 2D descriptors were being used to develop the model. The QSAR model is able to predict the pIC_{50} and could be used as a prediction tool for compounds having the same skeletal framework. Molecular docking was done for all compounds using homology model of α-glucosidase to identify important binding modes responsible for inhibition activity.

1. Introduction

Diabetes mellitus is a disease involving metabolic disorder resulting from defects in insulin secretion and action. This result in increase of blood glucose level (hyperglycemia) and causes dysfunction to important organs like blood vessels and nerves [1]. Study shows that the number of diabetes mellitus patients increases each year. The trend displayed that patient with diabetes increases from 153 million to 347 million between the year 1980–2008 [2]. Based on World Health Organization (WHO) projection, diabetes is predicted to become the seventh leading cause of death worldwide by 2030. One of the approaches, which can be taken to reduce diabetes is to inhibit enzymes like α-glucosidase by controlling the postprandial glucose levels and suppressing postprandial hyperglycemia [3].

Inhibitors for α-glucosidase function by reversibly inhibit digestive α-glucosidase that retards glucose liberation from complex starch and carbohydrate. This results in delay for glucose to be absorbed into bloodstream and, therefore, decreases plasma glucose level. Inhibition of a-glucosidase has attracted plenty of interest by pharmaceutical industry as a treatment method of

* Corresponding author. Atta-ur-Rahman Institute for Natural Product Discovery, Universiti Teknologi MARA, Puncak Alam Campus, 42300, Selangor D.E., Malaysia.
** Corresponding author. Atta-ur-Rahman Institute for Natural Product Discovery, Universiti Teknologi MARA, Puncak Alam Campus, 42300, Selangor D.E., Malaysia.
E-mail addresses: taha_hej@yahoo.com, muhamm9000@puncakalam.uitm.edu.my (M. Taha), norhadiani@puncakalam.uitm.edu.my (N.H. Ismail).

http://dx.doi.org/10.1016/j.ejmech.2015.10.017
0223-5234/

diseases like diabetics, viral infections, hepatitis, and cancer [4–6]. Inhibitors for α-Glucosidase are found to show antitumor, antidiabetic, antiviral, and immunoregulatory activities [7–9]. Research on α-glucosidase inhibitors such as castanospermine, *N*-butyl-deoxynojirimycin and deoxynojirimycin showed that they are potent against HIV replication [10].

Currently, glycosidic based α-glucosidase inhibitors such as miglitol [11], voglibose [12], acarbose [13] and nojirimycin [14] are used to control glucose level in blood of diabetic patients. Despite being potent, these inhibitors have some limitations such as diarrhea, abdominal distension, meteorism and flatulence [15]. Acarbose, deoxynojirimycin, miglitol, and voglibose are among the key known candidates which are used extensively to inhibit α-glucosidase activity. Due to side effects and absorptivity problems associated with these inhibitors [16,17], new potent α-glucosidase inhibitors are highly desired. Hence, a lot of efforts have been put in to design and develop non-glycosidic based inhibitors for safer [18] and effective α-glucosidase inhibitors [19].

α-Glucosidase (EC3.2.1.20) is an enzyme commonly found in small intestine. α-Glucosidase hydrolyzes carbohydrates and produces α-D-glucose during food digestion. Carbohydrates and α-D-glucose that has been produced are being absorbed into blood stream, thus increases postprandial blood glucose level and leads to diabetes. Therefore, α-glucosidase inhibitors are of significant importance to control diabetes since they could reduce carbohydrate digestion and monosaccharide absorption [20,21]. Glucose concentration in blood is extremely critical for diabetes mellitus management and it must be between an acceptable ranges (70–100 mg/dl) [22]. In addition to preventing diabetes, blood glucose level which is controlled may avoid hyperlipoproteinemia, obesity, and hyperlipidemia [23].

α-Glucosidase also enables monosaccharide removal from viral glycoproteins, thus, its inhibitors could alter cell-to-cell signaling, virus recognition by the cell and could be used in the treatment of viral diseases, cancer, and immune-regulations [24–28].

Flavone is one of the class of flavonoids that is present in fruits and vegetables. Flavones are being consumed in daily diet and they improve health without giving any major side effect [29]. In order to explore diverse roles of flavones, investigating various methods for their synthesis and structural modification of flavones ring has now become important goals of several research groups. Thus, naturally obtained flavone moiety having a variety of biological activities can be taken as lead compound for the synthesis of semi- and purely synthetic flavone derivatives with different functional groups at different positions of flavone skeleton.

Flavone scaffold is an important structure found in many pharmaceutically active compounds. They are structurally diverse and possess a variety of biological activity. This reason has increased the interest of medicinal chemists to further study flavones as lead molecules to treat various diseases. Recently, researchers had focused a lot on flavonoids bioactivities like free radicals scavenging ability and protection against peroxidation of lipid [30,31]. Researchers also showed interest in some flavonoids due to their ability to modulate NADPH oxidase activity and endothelial nitric oxide metabolism [32–38]. Various research indicate that flavonoids could reduce hyperglycemia, improve sensitivity and enhance secretion of insulin [39]. It has been established that flavonoids like kaempferol, luteolin, apigenin, chrysin and baicalein have the capability of inhibiting α-glucosidase activity [40,41], taking into consideration of the importance of ring A, B, and C towards the inhibition of α-glucosidase activity.

Benzohydrazides had been reported to possess various biological activities, which includes antileishmanial [42], antioxidant [43], antiglycation [44], antibacterial [45], and α-glucosidase inhibition [46] activities. In this paper, flavone derivatives possessing hydrazone linkage synthesized and evaluated for their α-glucosidase inhibition activity. We attempted to rationalize the effect of various substituents at different position on the inhibitory effect in terms of how the molecules bind with α-glucosidase protein.

2. Result and discussion

2.1. Chemistry

The title compounds were synthesized through Schemes 1 and 2. Flavone hydrazones **5**–**34** (Table 1) were synthesized through a single step reaction of 4-(4-oxo-4H-chromen-2-yl)benzohydrazide **4** with appropriate aryl aldehydes, in the presence of catalytic amount of glacial acetic acid. Compound **4** which is the key intermediate for the synthesis of target compounds **5**–**34** was prepared through a four-step sequence. Initially 2'-hydroxyacetophenone undergoes Aldol condensation with 4-formylbenzoic acid using aqueous KOH in ethanol to form (*E*)-4-(3-(2-hydroxyphenyl)-3-oxoprop-1-en-1-yl)benzoic acid **1**. Chalcone **1** was cyclized into flavone through oxidative cyclization by using well-known I_2-DMSO mixture as the oxidizing agent. Carboxylic acid of the resulting product **2** was converted into ester **3** before finally reacted it with hydrazine to form compound **4**.

The structure of newly synthesized compounds were confirmed by the various analytical techniques, ^{1}H NMR, ^{1}3C NMR, IR, MS and elemental analysis. All spectral data were in accordance with assumed structures. In the ^{1}H NMR spectra of chalcone **1,** olefinic protons H_α and H_β (Fig. 1) appeared as doublets at 7.86 ppm and 8.12 ppm respectively. The formation of chalcone **1** having *trans* conformation was verified using the coupling constant values (15.6 Hz) of both vinyl hydrogens (H_α and H_β). Oxidation of chalcone **1** leads to the formation of flavone **2** which involves removal of hydrogen from hydroxyl group and H_β. This was being confirmed through several changes to the ^{1}H NMR spectra. Splitting produced by vinylic protons (H_α and H_β) were no longer observed. This deduction was further confirmed by the appearance of singlet proton at 7.13 ppm representing H_α on the chromone ring.

2.2. In-vitro α-glucosidase inhibition

In continuation of our work on enzyme inhibition [47], we had synthesized compounds **1**–**34** and evaluate them for their α-glucosidase inhibition activity. The assay was carried out using baker's yeast α-glucosidase (EC 3.2.1.20). The result in Table 2 showed, with the exception of compound **3**, the compounds synthesized in this study are more active than the standard drug. Compounds **1** to **4**, which are the intermediate compounds for synthesis of the final compounds **5**–**34** were also evaluated for their inhibition activity. Comparison between results for intermediates **1** and **2** showed that flavone **2** has better activity as compared to chalcone **1**. This result indicates that the chromone moiety is playing a significant role in inhibiting the enzyme activity. Conversion of carboxylic acid to hydrazide **3** enhances the inhibition activity. Converting hydrazide **4** into hydrazones **5**–**34** further improves the inhibition activity. Comparison between results for intermediate compounds **1**–**4** with flavone-hydrazone derivatives **5**–**34** showed a significant improvement in the inhibitory activity, which indicates the importance of hydrazone linkage in inhibiting α-glucosidase activity. Compounds having hydroxyl, chloro and fluoro substituent showed potent activity with IC_{50} ranging between 15.4 and 86.3 μM while the other compounds having methyl, methoxy, nitro and bromo substituent are weakly active. Compounds **28**, **29** and **30** that are having pyridine ring also showed weak inhibitory activity against α-glucosidase. In order to understand further the effect of structural features and mechanism of

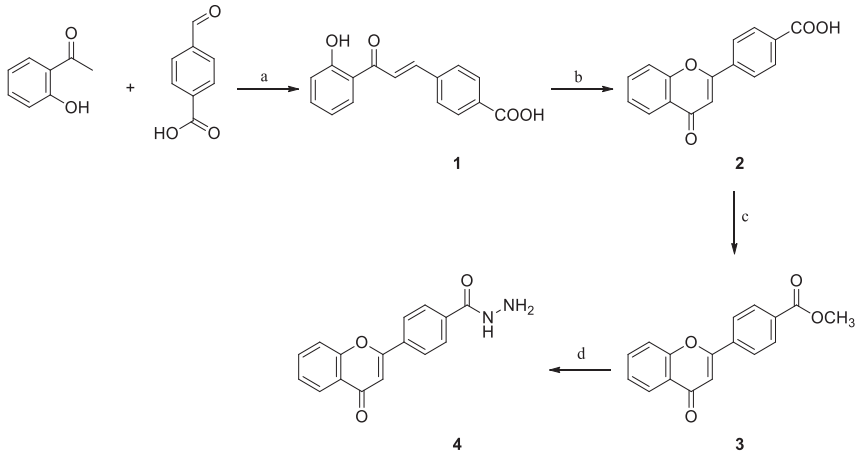

Scheme 1. Reaction scheme for synthesis of compound **4**. Reagents and condition: (a) Ethanolic-KOH, room temperature; (b) I_2-DMSO, reflux; (c) MeOH, H_2SO_4, reflux; (d) Hydrazine hydrate, MeOH, reflux.

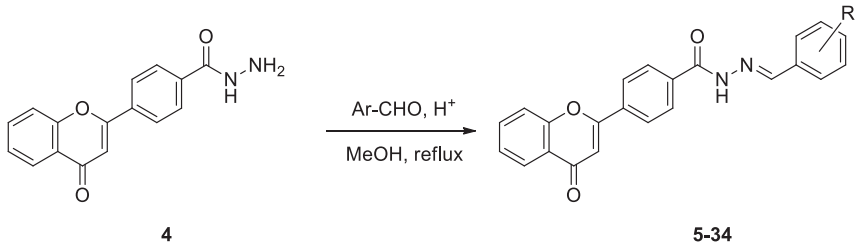

Scheme 2. Reaction scheme for synthesis of flavone hydrazones **5**–**34.**

action, the compounds were subjected through 2D QSAR and docking studies, which studies enable us to identify key structural features responsible for the inhibition activity as well as rationalizing the best binding modes in the active site of α-glucosidase. The compounds were not showing any activity against histone deacetylase inhibition and cytotoxicity activity.

2.3. 2D QSAR study

2.3.1. QSAR model development and validation

Quantitative structural activity relationship (QSAR) for α-glucosidase inhibition activity was performed to determine the factors/descriptors which correlates the bioassay results obtained with flavone derivatives (**5**–**34**), and to determine structural features contributing towards the inhibition activity. In this study, the compounds for training set and test set were selected using "cluster analysis" protocol in Discovery Studio 2.5. Cluster selection was done by allowing cluster to have fixed number of compounds for each cluster. Compounds selection was done using predefined set consisting of items such as AlogP, molecular weight, number of hydrogen donors and acceptors. The training set consisting of 21 compounds from the newly synthesized flavone hydrazones together with their measured pIC_{50} ($-logIC_{50}$) was used to develop the QSAR model. The molecular properties for the compounds in the training set were calculated using "Calculate Molecular Properties" protocol. The protocol includes calculation for 2D molecular properties, energies of highest occupied and lowest unoccupied molecular orbitals (HOMO and LUMO) for compounds of the

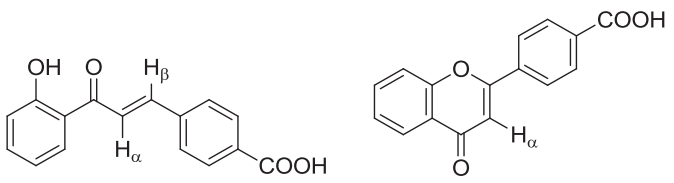

Fig. 1. Representation of H_α and H_β of chalcone **1** and flavone **2**.

Table 1
Synthesis of flavone hydrazone derivatives **5**–**34**.

Compound	R
5	2,4,6-OH
6	2,3-OH
7	2,4-OH
8	2,5-OH
9	3,4-OH
10	2-OH
11	3-OH
12	4-OH
13	2-OH, 4-OCH_3
14	3-OH, 4-OCH_3
15	2-OH, 5-OCH_3
16	3,5-OCH_3
17	2-Br, 4-OH
18	2-CH_3
19	3-CH_3
20	4-CH_3
21	2-Cl
22	3-Cl
23	4-Cl
24	2-NO_2
25	3-NO_2
26	4-NO_2
27	2-Fl
28	3-Fl
29	4-Fl
30	3-OCH_3
31	4-OCH_3
32	2-Pyr
33	3-Pyr
34	4-Pyr

Table 2
In-vitro α-glucosidase Inhibition Activity of Compounds **1**–**34**.

Compound	IC_{50} (μM ± SEM[a])	Compound	IC_{50} (μM ± SEM[a])
1	840 ± 2.50	**19**	497.4 ± 0.70
2	802.6 ± 1.34	**20**	367.4 ± 0.54
3	N.A.[b]	**21**	29.6 ± 0.26
4	730 ± 0.50	**22**	64.5 ± 2.08
5	15.4 ± 0.22	**23**	38.3 ± 0.34
6	16.9 ± 0.65	**24**	123.4 ± 1.69
7	27.3 ± 0.36	**25**	98.0 ± 1.10
8	37.8 ± 0.44	**26**	88.4 ± 0.97
9	17.2 ± 1.21	**27**	17.1 ± 0.24
10	37.4 ± 0.50	**28**	22.8 ± 1.23
11	86.3 ± 0.98	**29**	19.4 ± 0.20
12	27.4 ± 1.46	**30**	680.5 ± 1.27
13	29.4 ± 0.32	**31**	690.3 ± 2.04
14	34.4 ± 1.18	**32**	487.4 ± 1.36
15	37.4 ± 0.33	**33**	520.7 ± 0.80
16	623 0.1 ± 0.61	**34**	430.2 ± 0.28
17	587.4 ± 1.42	**Acarbose**	**860.23 ± 6.10**
18	487.4 ± 1.08		

[a] SEM is the standard error of the mean.
[b] N.A. No activity.

training set. In this study, 2D descriptors like AlogP, molecular weight, number of hydrogen donor, and number of rotatable bonds were utilized in developing the model.

Notably, AlogP is a measure of the hydrophobicity of the molecule and calculated in Discovery Studio as the Log of the octanol–water partition coefficient, while Molecular Fractional Polar Surface Area is the ratio of the polar surface area divided by the total surface area of the molecule.

In this study, Multiple Linear Regression (MLR) analysis method was being used to obtain the model. Descriptors were selected based on the results of the intercorrelation matrix between the descriptors, which should intercorrelate more than 0.6. Descriptors that were selected for this study have intercorrelation values lower than 0.5 (Table 3a) to prevent model overfitting. These value also showed that these descriptors are independent. Robustness of the established QSAR models were verified using Leave-one-out (LOO) internal validation or cross-validation (q^2), where r^2 (squared correlation coefficient value) equals 0.848, while the r^2 (pred), which is equivalent to q^2 from a leave-one-out cross validation, is 0.705 (Table 3b).

In addition, validation was done by measuring the residuals between the experimental and the predicted activity of the training set (Table 4). A correlation plot representing the correlation between predicted pIC_{50} against experimental pIC_{50} of test set (Fig. 2b) showed that the plot has a regression correlation coefficient (r^2) of 0.783, which is considered quite good. Despite showing good correlation, the QSAR model can be further improved to be used applied for prediction of more effective hits having the same skeletal framework.

2.3.2. 2D QSAR model analysis

Equation (1) represents the model obtained using Multiple Linear Regression and it is graphically visualized using a scatter plot of predicted pIC_{50} against experimental pIC_{50} values for the training set and test set compounds as shown in Fig. 2. Equation (1) describes that α-glucosidase inhibition activity of flavone derivatives **5**–**34** are affected by four descriptors, which are AlogP, molecular weight, number of hydrogen bond donor, and number of rotatable bonds. Comparison between descriptors in the equation showed that AlogP, number of hydrogen bond donor, and number of rotatable bonds are among those which contributed significantly towards the high correlation as compared to molecular weight. Despite showing some effect on the pIC_{50}, small molecular variation that only involves substitution on the extended benzylidene ring has affected the molecular weight descriptor. Having the lowest constant value, the equation suggest that small changes in molecular weight could slightly affect the IC_{50} value as compared to the other descriptors. Based on the equation, it was observed that increasing the number of rotatable bonds descriptor, which has the highest constant value, in the molecule could significantly increase the pIC_{50} value and, therefore, gives a lower IC_{50}. However, other descriptors in the equation, which are AlogP and molecular weight, suggest that increasing the lipophilicity and molecular weight of the compounds will only reduce the pIC_{50} value and gives a higher IC_{50} value. This observation supports the actual activity which

Table 4
Experimental activity of the synthesized hybrids against the predicted activity according to Equation (1).

Compound	Experimental activity (−log IC_{50})	Predicted activity (−log IC_{50})	Residual
11	−1.936	−1.445	−0.491
13	−1.468	−1.539	0.071
15	−1.572	−1.539	−0.034
18	−2.688	−2.632	−0.056
19	−2.696	−2.632	−0.065
24	−2.091	−1.957	−0.134
27	−1.240	−1.313	0.073
28	−1.350	−1.313	−0.037
33	−2.717	−2.684	−0.032

Table 3
a) Intercorrelation data of descriptors used to develop QSAR Model Equation 1 and b) Regression statistics table.

a)

	pIC_{50}	ALogP	Molecular_Weight	Num_H_Donors	Num_RotatableBonds
pIC50	1	−0.034	0.265	0.271	−0.221
ALogP		1	0.343	−0.422	0.032
Molecular_Weight			1	0.502	0.237
Num_H_Donors				1	−0.192
Num_RotatableBonds					1

b)

Statistic	Value
N	21
r	0.921
R2	0.848
r^2 (Adjusted)	0.840
r^2 (predicted)	0.705
Least-squared Error	0.198

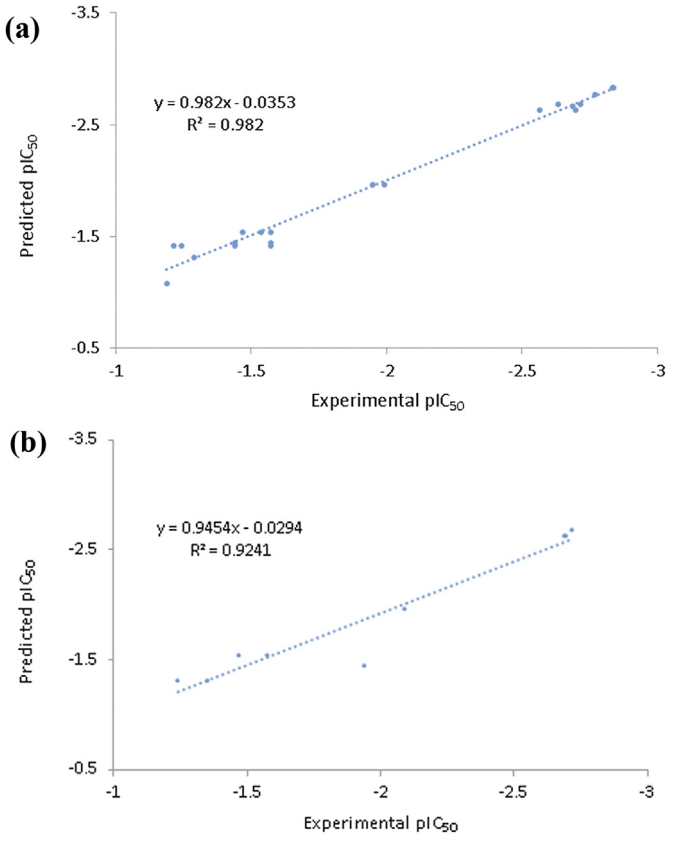

Fig. 2. Predicted versus experimental pIC_{50} of the (a) training set and (b) test set against α-glucosidase.

showed that adding rotatable and non-polar substituents methyl and methoxy substituent to compounds could increase the lipophilicity and molecular weight of the compounds and will significantly reduce the pIC_{50} value to give a higher IC_{50} value. On the other hand, the equation also suggest that increasing the number of hydrogen bond donor could increases the activity of the compounds by lowering the IC_{50} value, which also supports the general observation results from *in-vitro* activity, which show that increasing hydroxyl group in the structure could enhance the activity by giving lower IC_{50} value. Docking results further validate this QSAR model by taking into accounts the effect of all descriptors used in this model.

Equation 1. Equation representing the QSAR model;

$$pIC_{50} = -16.827 - 0.509\,(\text{AlogP}) - 5.819 \times 10^{-2}\,(\text{Molecular\_Weight}) + 0.213\,(\text{Num\_H\_Donors}) + 1.334\,(\text{Num\_RotatableBonds}) \quad (1)$$

2.4. Docking study

Molecular docking was performed on all flavones derivatives (**5**–**34**) to identify possible binding mode which explains the reason for their potency. Since crystal structure for α-glucosidase of *Saccharomyces cerevisiae* is still not available, docking study was conducted using a homology model for α-glucosidase. Preliminary results on sequence analysis of α-glucosidase from *S. cerevisiae* showed that the most suitable template for homology modeling is isomaltase (EC 3.2.1.10, oligo-1,6-glucosidase, MALX3) (PDB ID: 3A4A) from baker's yeast which shares 71% identity and 84% similarity with the target enzyme, α-glucosidase of *S. cerevisiae*. Sequence analysis on the homology model's sequence showed high sequence homology with the target enzyme. The active site contains important and highly conserved amino acids amino acids (Fig. 3) [48]. The final structure of α-glucosidase generated from homology modeling was evaluated using PROCHECK. The Ramachandran plot obtained from PROCHECK showed that 87.5% of residues of the final 3D structure lied in most favored regions (Fig. 4).

Prior to docking and analysis of the binding mode of the most active compound **5**, the docking method was validated through control docking of native inhibitor. Acarbose was docked into α-glucosidase from Sugar beet (PDB code: 3W37) and compared by superimposing with the native ligand in the protein (Fig. 5a). The rmsd value between docked and actual pose of acarbose was found to be 0.65 Å. Even though α-glucosidase from Sugar beet share relatively low homology with baker's yeast α-glucosidase (16% identity), the active site is highly conserved and main interactions of the ligand remain the same [48]. Another control docking was done on the target protein, isomaltase from Baker's yeast, using α-D-glucopyranose which is the native ligand located in the active site (Fig. 5b). The rmsd value for docked pose and native ligand was found to be 0.93 Å.

All flavones were docked and aligned in the binding pocket. Based on docking results of the aligned molecules (Fig. 6), the benzylidene moiety of the compounds are oriented towards the core of the binding pocket. This enables the substituents on the benzylidene moiety to interact closely with important residues in the active site. Introduction of hydrophilic substituents with H-bond donating properties like hydroxyl groups on the benzylidene moiety showed the most interaction with active residues which led to extra interactions and increase of the activity. Benzohydrazone linkage provides torsional degree of freedom (rotatability) that substantially decreases the entropic penalty for the formation of enzyme–inhibitor complex. This feature validates one of the descriptors used in the QSAR model, which suggest that increase in number of rotatable bonds could enhance the inhibition activity. Four hydrogen bonds are established between the phenolic and carbonyl oxygen of compound **5** and the side chains of His239, His245, His279, and Thr275. Benzohydrazone moiety resides in close proximity to the catalytic residues including Asp214, Glu276, His348, and Asp349, indicating that it can serve as surrogate for the terminal glucose in the substrate.

The main flavone scaffold of all derivatives (**5**–**34**) are better aligned when compared to the benzylidene moiety. The flavone scaffold which is positioned in a hydrophobic pocket allows formation of highly stable complexes. Several observations were made based on the interaction of flavone moiety with the enzyme. The main interaction which played the most significant role in stabilizing the enzyme–inhibitor complex is the interaction of benzopyrone ring of flavone moiety with Phe311 and Lys155 through a Pi–Pi stacking and Pi-cation interaction, respectively. Ring B of flavone forms additional Pi–Pi stacking with Phe311.

Two hydrogen bonds were observed for the most active compound, **5**, in the series (Fig. 7a). Besides forming pi-cation interaction, NH fragment of Lys155 also forms hydrogen bonding with oxygen of the ether linkage on ring C which further stabilizes the enzyme inhibitor complex. On the other hand, hydroxyl forms hydrogen bonding with catalytic residue His279, which is believed to have some reducing effect in the enzyme's activity. In Fig. 6b, nitrogen of benzohydrazone backbone forms a Pi-cation interaction with another catalytic residue His239.

Attempt to validate the QSAR model using docking results showed a high degree of correlation in terms of substituent's lipophilicity, ability to form hydrogen bonding, and rotatability. Docking studies showed that increase in number of hydrogen bond allows more interaction to form between active residues and the ligand. This observation satisfy the number of hydrogen bond

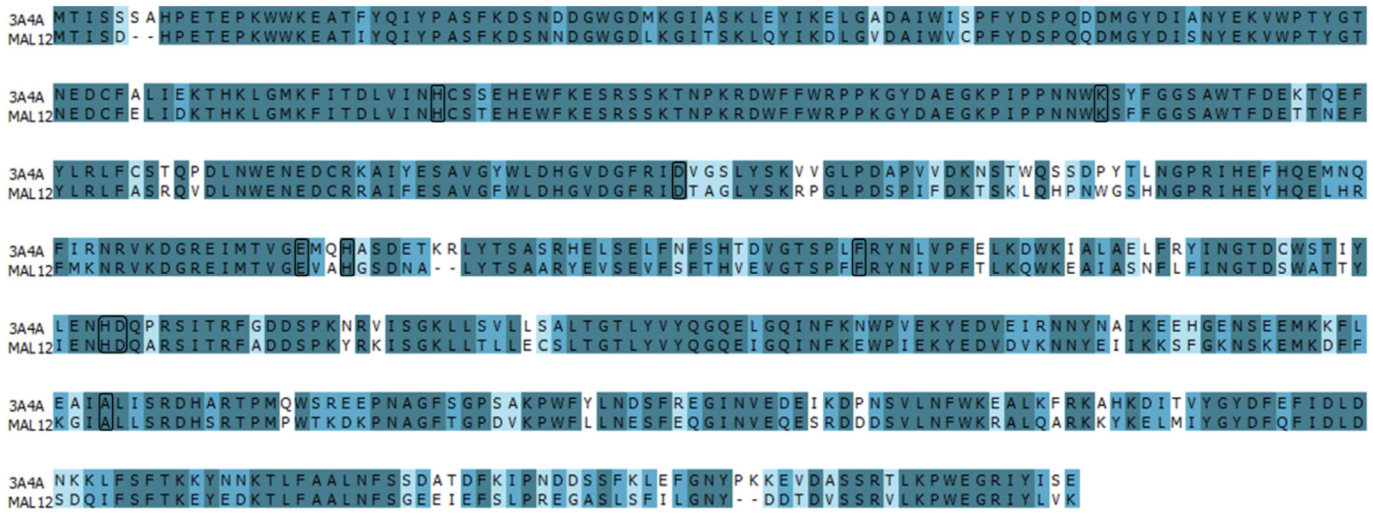

Fig. 3. Sequence analysis between 3A4A and MAL12 showing high sequence homology of important catalytic residues monitored throughout docking studies.

donor descriptor, which was observed to reduce the IC_{50} value when number of hydroxyl substituent was increased. In a different observation, it is also clearly visualized that increasing lipophilicity properties of the substituents by replacing hydroxyl with methoxy substituents causes shifting of benzylidene ring and prevents optimal interaction from taking place. Inhibition activity also decreases due to steric hindrance imposed by methoxy and inability to function as a hydrogen bond donor. The effect from steric hindrance by methoxy is visualized in Fig. 8c and d. Compounds **14** and **15**, which contains both hydroxyl and methoxy substituents, displayed better activity as compared to compounds **30** and **31** which are single substituted with methoxy substituent. For compounds **14** and **15**, the hydroxyl groups for both compounds are oriented towards the hydrophilic pocket (Fig. 8a and b). It was observed that substituents for both compounds **14** and **15** are not capable of interacting with any catalytic residues due to steric hindrance imposed by methoxy substituent. For compound **14**, methoxy group forms hydrogen bonding with Thr217, while for compound **15**, hydroxyl group interacts with Asn241.

Eventhough the activity for compound **14** and **15** are considered quite good, hydrogen bond between methoxy of compound **14** and hydroxyl of compound **15** were not enough to increase the activity in a significant way. Rather than adding more hydroxyl substituents, it seems more important to place hydroxyl substituents on *N*-benzylidene ring at the correct position for the compounds to be able to inhibit α-glucosidase activity.

3. Conclusion

All flavone-hydrazones synthesized in this study are active in inhibiting α-glucosidase. The result strongly suggest that chromone moiety and hydrazone linkage played important role in suppressing the activity of α-glucosidase activity as the activity of all the compounds improve significantly as compared to the starting material **4**. 2D QSAR model established showed correlation and contribution of various structural features in the activity. Descriptors such as AlogP, number of H bond acceptor/donor, molecular weight, and number of rotatable bonds are statistically important in this study. AlogP and number of rotatable bonds play an important role as compared to other descriptors like H-bond donors and molecular weight. QSAR equation suggest that by increasing number of hydrogen bond donor, molecular weight, and number of rotatable bonds, the inhibition activity could be improved. The validated QSAR model is suitable to predict α-glucosidase inhibition activity for compounds having similar skeletal structure in the future. Docking studies showed that benzopyrone ring of flavone moiety that is located in hydrophobic pocket stabilizes the enzyme–inhibitor complex by forming Pi–Pi stacking with Phe311 and Pi-cation interaction with Lys155. *N*-benzylidene moiety resides in close proximity to catalytic residues like Asp214, Glu276, His348, and Asp349 indicates that it can serve as a surrogate for terminal glucose in α-glucosidase. On the other hand, benzohydrazone linkage provides torsional degree of freedom in terms of its rotatablility, which had substantially decreased the entropic penalty for the formation of enzyme–inhibitor complex. Phenolic and carbonyl oxygens of compound **5,** which is the most active derivative, forms 4 hydrogen bonds with side chains of His239, His245, His279, and Thr275. Therefore, the compounds are most likely to be capable of inhibiting the catalytic action of α-glucosidase by a tight binding in the active site through the multiple hydrogen bond and hydrophobic interactions in a cooperative fashion. In addition to a-glucosidase inhibition activity, the compounds were also tested for their cytotoxicity and ability to inhibit histone deacetylase. It was found that they do not show any activity for histone deacetylase inhibition and cytotoxicity activity.

4. Experimental

4.1. Chemistry

Melting points were determined using Sinosource SGW X-4 melting point apparatus with microscope (Guangzhou, China). IR spectra obtained using PerkinElmer Spectrum 100 FTIR Spectrometer (Waltham, MA, USA) equipped with a diamond crystal Attenuated Total Reflectance (ATR) accessory by PIKE Technologies (Madison, WI, USA). NMR spectroscopy was obtained using Bruker Ultra Shield FT NMR 500 MHz and Avance III 600 Ascend spectrometer (Wissembourg, France). EI-MS spectroscopic analysis had been obtained using Finnigan-MAT-311-A instrument (Bremen, Germany). Thin layer chromatography (TLC) was performed using precoated silica gel plates (Merck, Kieselgel 60 F-254, 0.20 mm).

4.2. Synthesis of (E)-4-(3-(2-hydroxyphenyl)-3-oxoprop-1-en-1-yl) benzoic acid (*1*)

In a 250 ml flask, 2′-hydroxyacetophenone (30 mmol) was being

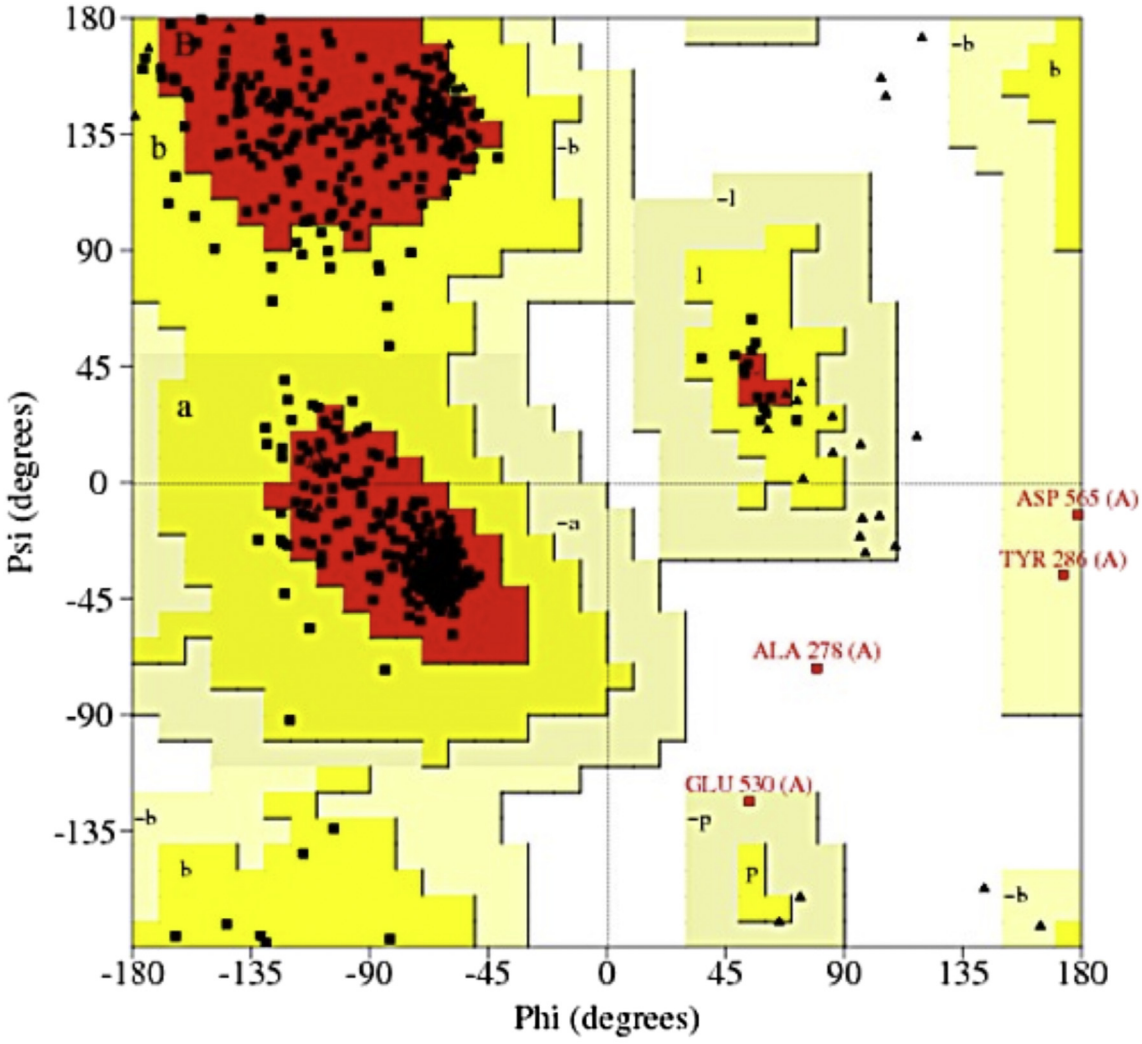

Plot statistics

Residues in most favoured regions [A,B,L]	448	87.5%
Residues in additional allowed regions [a,b,l,p]	60	11.7%
Residues in generously allowed regions [~a,~b,~l,~p]	3	0.6%
Residues in disallowed regions	1	0.2%
Number of non-glycine and non-proline residues	512	100.0%
Number of end-residues (excl. Gly and Pro)	2	
Number of glycine residues (shown as triangles)	37	
Number of proline residues	28	
Total number of residues	579	

Fig. 4. Ramachandran plot for homolog model of 3A4A.

mixed with 4-formylbenzoic acid (30 mmol). The mixture was dissolved in 100 ml of 15% (w/v) sodium hydroxide in ethanol and stirred at room temperature. Reaction progress was monitored using TLC and upon completion, diluted sulphuric acid was added to allow precipitation. The precipitate was filtered and crystallized in ethanol to afford pure product. Yellow solid; yield 78%; m.p. 250–252 °C; IR (ATR) cm^{-1}: 2990, 2831, 1678, 1643, 1568, 1291; ^1H NMR (600 MHz, DMSO-*d6*): δ 7.02–7.05 (m, 2H), 7.58 (t, $J = 7.2$ Hz, 1H), 7.86 (d, $J = 15.6$ Hz, 1H), 8.00–8.05 (m, 4H), 8.13 (d, $J = 15.6$ Hz, 1H), 8.24 (d, $J = 7.5$ Hz, 1H), 11.15 (s, 1H), 12.36 (s, 1H); ^{13}C NMR (125 MHz, DMSO-*d6*): δ 117.7, 119.5, 120.9, 122.3, 126.3, 126.3, 128.6, 130.6, 130.6, 133.5, 135.5, 137.5, 143.3, 161.4, 168.5, 193.5; Anal. Calcd for $C_{16}H_{12}O_4$: C = 71.64, H = 4.51, Found: C = 71.63, H = 4.52; EI MS *m/z* (% rel. abund.): 268.07 (M^+, 68.2%).

4.3. Synthesis of 4-(4-oxo-4H-chromen-2-yl)benzoic acid (**2**)

Compound **1** (22.4 mmol) was mixed with iodine (0.23 mmol). The mixture was dissolved in 50 ml of DMSO and refluxed at 170 °C. After 3 h, sodium thiosulfate was added to the reaction mixture followed by excess amount of water to allow precipitation. The product was rinsed and allowed to dry at room temperature to

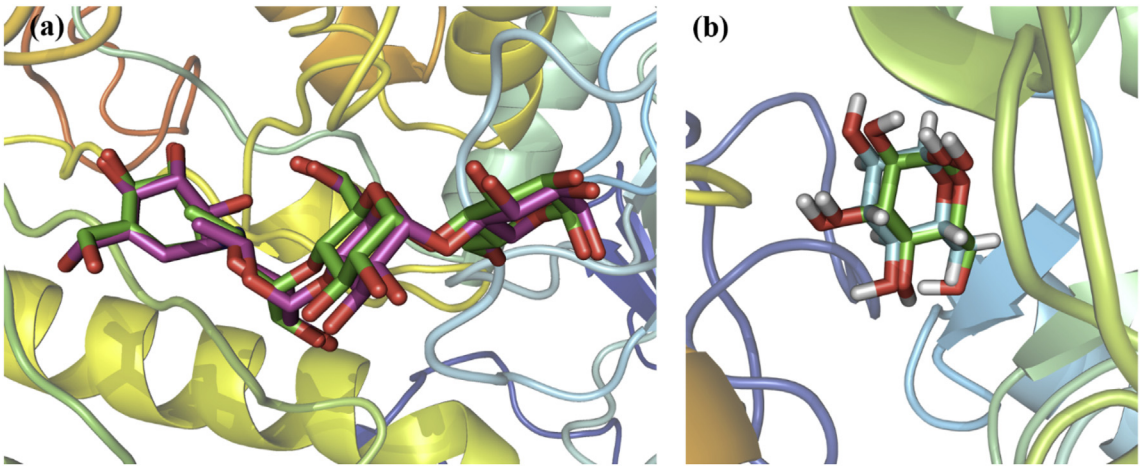

Fig. 5. Superimpose of (a) acarbose in 3W37 and (b) α-D-glucopyranose in 3A4A.

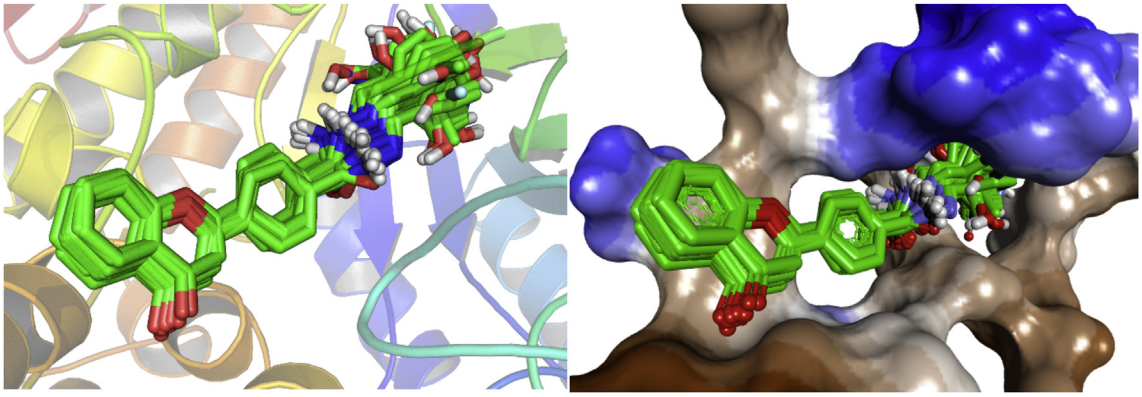

Fig. 6. Flavone derivatives (**5**–**34**) aligned in the binding pocket.

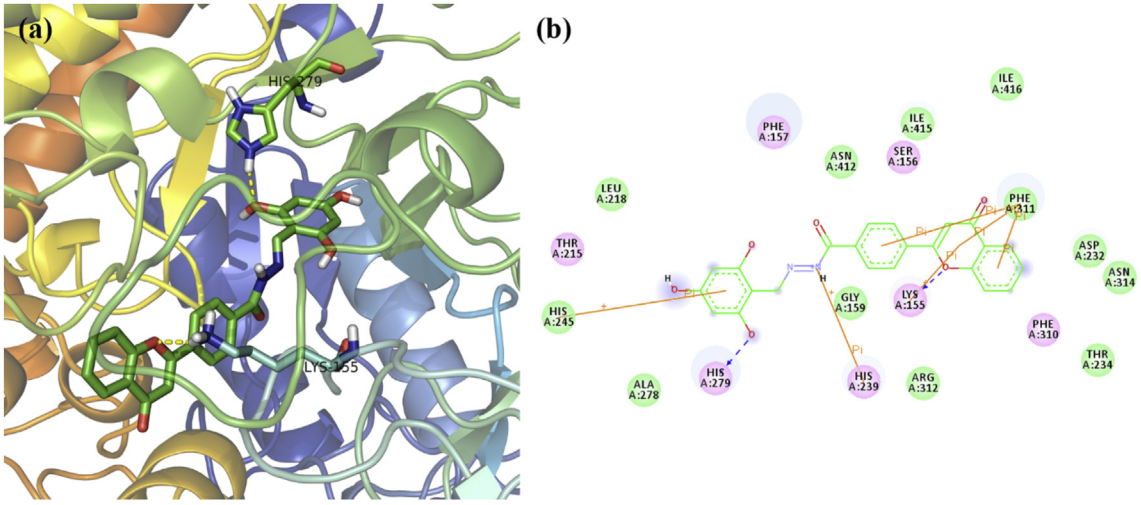

Fig. 7. (a) Docking of the most active compound **5** and (b) its 2D interaction diagram.

afford pure product. Light yellow solid; yield 90%; m.p. 298–300 °C; IR (ATR) cm^{-1}: 3420, 3081, 2885, 1707, 1623, 1588, 1567, 1415, 1242; ^{1}H NMR (500 MHz, DMSO-*d6*): δ 7.13 (s, 1H), 7.51(t, $J = 7.5$ Hz, 1H), 7.80 (d, $J = 8.5$ Hz, 1H), 7.84 (t, $J = 7.0$ Hz, 1H), 8.05 (d, $J = 8.0$ Hz, 1H), 8.09 (d, $J = 8.5$ Hz, 2H), 8.22 (d, $J = 8.5$ Hz, 2H), 12.21 (s, 1H); ^{13}C NMR (125 MHz, DMSO-*d6*): δ 105.9, 118.4, 124.6, 124.6, 124.9, 125.7, 126.0, 128.9, 130.3, 130.3, 132.6, 134.4, 156.8, 163.7, 168.8, 178.0; Anal. Calcd for $C_{16}H_{10}O_4$: C = 72.18, H = 3.79, Found: C = 72.19, H = 3.81; EI MS *m/z* (% rel. abund.): 266.06 (M^+, 73.6%).

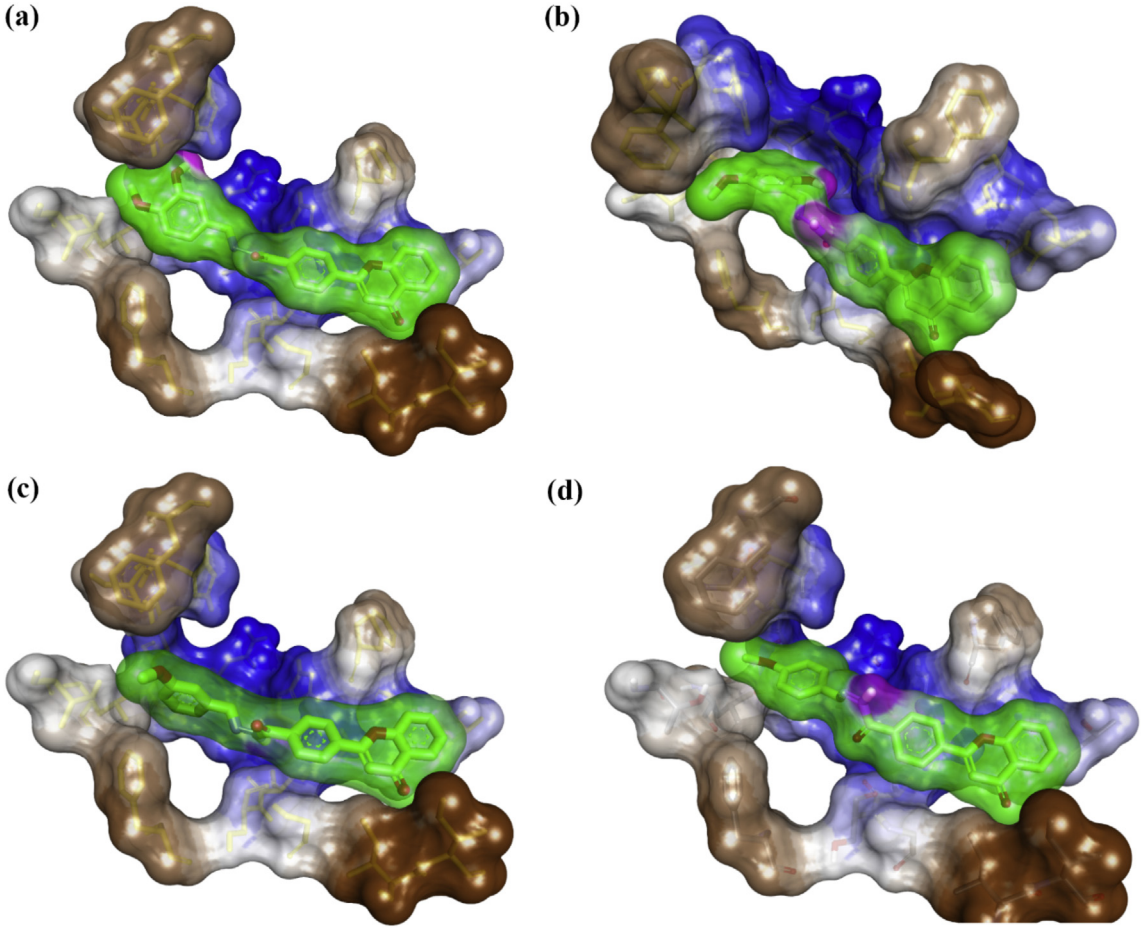

Fig. 8. Hydrophobic and steric surfaces of (a) compound **14**, (b) compound **15**, (c) compound **30** and (d) compound **31**.

4.4. Synthesis of methyl 4-(4-oxo-4H-chromen-2-yl)benzoate (**3**)

Compound **2** (18.8 mmol) was mixed with 1 ml of concentrated sulphuric acid and dissolved in 100 ml methanol. The reaction was refluxed for more than 16 h and monitored using TLC. Upon completion, methanol was being removed using rotavap. Residue was collected and rinsed using excessive amount of water and crystallized in methanol to afford pure product. White solid; yield 95%; m.p. 268–270 °C; IR (ATR) cm^{-1}: 3325, 3073, 2873, 1742, 1707, 1648, 1556, 1412, 1262; ^{1}H NMR (500 MHz, DMSO-*d6*): δ 3.91 (s, 3H), 7.16 (s, 1H), 7.52(t, J = 7.0 Hz, 1H), 7.82 (d, J = 8.0 Hz, 1H), 7.86 (t, J = 7.0 Hz,1H), 8.07(d, J = 8.0 Hz, 1H), 8.13(d, J = 8.5 Hz, 2H), 8.27(d, J = 8.5 Hz, 2H); ^{13}C NMR (125 MHz, DMSO-*d6*): δ 55.6, 105.91, 118.2, 124.7, 125.1, 125.1, 125.7, 126.5, 128.2, 128.2, 131.0, 131.5, 133.2, 156.8, 163.7, 167.4, 178.0; Anal. Calcd for $C_{17}H_{12}O_4$: C = 72.85, H = 4.32, Found: C = 72.87, H = 4.35; EI MS *m/z* (% rel. abund.): 280.07 (M^+, 76.3%).

4.5. Synthesis of 4-(4-oxo-4H-chromen-2-yl)benzohydrazide (**4**)

Compound **3** (17.7 mmol) was dissolved in 100 ml methanol containing 25 ml hydrazine hydrate. The reaction mixture was refluxed for at least 6 h. Reaction progress was monitored using TLC. Methanol was removed using rotavap and product was rinsed with plenty of water. The product was rinsed and allowed to dry at room temperature to afford pure product. White solid; yield 88%; m.p. 197–199 °C; IR (ATR) cm^{-1}: 3327, 3139, 2997, 1630, 1558, 1469, 1341, 1251; ^{1}H NMR (500 MHz, DMSO-*d6*): δ 4.51 (s, 2H), 6.91 (t, J = 7.5 Hz, 1H), 6.96 (d, J = 7.5 Hz, 1H), 7.19 (t, J = 7.0 Hz, 1H), 7.33 (s, 1H), 7.74 (d, J = 7.5 Hz, 1H), 7.918 (s, 4H), 9.82 (s, 1H); ^{13}C NMR (125 MHz, DMSO-*d6*): δ 105.8, 118.3, 124.3, 124.8, 125.2, 125.6, 125.6, 126.3, 126.3, 133.8, 137.3, 137., 157.2, 163.3, 167.4, 178.2; Anal. Calcd for $C_{16}H_{12}N_2O_3$: C = 68.56, H = 4.32, N = 9.99, Found: C = 68.57, H = 4.34, N = 9.97; EI MS *m/z* (% rel. abund.): 280.17 (M^+, 58.2%).

4.6. General procedure for synthesis of flavone hydrazones (**5**–**34**)

Compound **4** (0.5 mmol) and substituted benzaldehydes (0.5 mmol) were being mixed with 1 ml of glacial acetic acid in a 50 mL round bottom flask. The mixture was being dissolved in 20 mL of methanol and refluxed. Progress monitored using TLC and upon completion, solvent was being removed using rotary evaporator. Product was collected and rinsed with diethyl ether to afford pure product.

4.6.1. (E)-4-(4-oxo-4H-chromen-2-yl)-N′-(2,4,6-trihydroxybenzylidene)benzohydrazide (**5**)

Light yellow solid; Yield 76%; m.p. 283–285 °C; IR (ATR) cm^{-1}: 3353, 3139, 2994, 1657, 1611, 1556, 1519, 1470, 1372, 1269, 1186, 760; ^{1}H NMR (500 MHz, DMSO-*d6*): δ 5.86 (s, 2H), 6.93 (t, J = 7.5 Hz, 1H), 6.93 (d, J = 8.0 Hz, 1H), 6.93 (t, J = 7.0 Hz, 1H), 7.38 (s, 1H), 7.75 (s, 1H), 7.99–8.04 (m, 4H), 8.83 (s, 1H), 9.85 (s, 1H), 11.13 (s, 2H), 11.94 (s, 1H); ^{13}C NMR (125 MHz, DMSO-*d6*): δ 95.8, 95.8, 105.5, 106.8, 118.2, 125.1, 125.4, 125.4, 125.6, 126.2, 126.8, 126.8, 133.7, 137.2, 138.8, 144.6, 156.2, 161.7, 161.7, 163.2, 163.5, 164.3, 178.1; Anal. Calcd for $C_{23}H_{16}N_2O_6$: C = 66.34, H = 3.87, N = 6.73, Found: C = 66.33,

H = 3.88, N = 6.71; EI MS *m/z* (% rel. abund.): 416.20 (M^+, 72.5%).

*4.6.2. (E)-4-(4-oxo-4H-chromen-2-yl)-N′-(2,3-dihydroxybenzylidene)benzohydrazide (**6**)*

White solid; Yield 81%; m.p. 288–290 °C; IR (ATR) cm^{-1}: 3373, 3159, 2835, 1609, 1539, 1469, 1357, 1257, 1186, 754; ^1H NMR (500 MHz, DMSO-*d6*): δ 6.75 (t, *J* = 7.5 Hz, 1H), 6.87 (d, *J* = 7.0 Hz, 1H), 6.92 (t, *J* = 7.5 Hz, 1H), 6.98 (d, *J* = 7.5 Hz, 2H), 7.20 (t, *J* = 7.0 Hz, 1H), 7.76 (s, 1H), 8.01–8.04 (m, 5H), 8.63 (s, 1H), 9.25 (s, 1H), 11.14 (s, 1H), 12.19 (s, 1H); ^{13}C NMR (125 MHz, DMSO-*d6*): δ 105.9, 118.2, 119.7, 119.9, 121.3, 122.0, 125.0, 125.2, 125.4, 125.4, 126.2, 126.9, 126.9, 133.9, 137.1, 138.7, 144.4, 146.4, 149.3, 155.9, 163.4, 164.5, 178.3; Anal. Calcd for $C_{23}H_{16}N_2O_5$: C = 69.00, H = 4.03, N = 7.00, Found: C = 69.01, H = 4.05, N = 6.98; EI MS *m/z* (% rel. abund.): 400.12 (M^+, 64.7%).

*4.6.3. (E)-4-(4-oxo-4H-chromen-2-yl)-N′-(2,4-dihydroxybenzylidene)benzohydrazide (**7**)*

Light yellow solid; Yield 88%; m.p. 294–296 °C; IR (ATR) cm^{-1}: IR (ATR) cm^{-1}: 3354, 3212, 3021, 1626, 1606, 1495, 1466, 1259, 1166, 749; ^1H NMR (500 MHz, DMSO-*d6*): δ 6.34 (s, 1H), 6.37 (d, *J* = 8.0 Hz, 1H), 6.91 (t, *J* = 7.5 Hz, 1H), 6.97 (d, *J* = 8.0 Hz, 1H), 7.20 (t, *J* = 7.5 Hz, 1H), 7.32 (d, *J* = 8.5 Hz, 1H), 7.36 (s, 1H), 7.75 (d, *J* = 7.0 Hz, 1H), 8.00–8.03 (m, 4H), 8.53 (s, 1H), 9.23 (s, 1H), 10.14 (s, 1H), 11.53 (s, 1H); ^{13}C NMR (125 MHz, DMSO-*d6*): δ 103.0, 105.9, 109.2, 113.1, 118.2, 125.1, 125.4, 125.4, 125.4, 126.2, 126.9, 126.9, 130.8, 133.9, 137.1, 138.7, 151.1, 156.2, 160.5, 160.5, 163.4, 164.3, 178.1; Anal. Calcd for $C_{23}H_{16}N_2O_5$: C = 69.00; H = 4.03; N = 7.00; Found: C = 69.02; H = 4.04; N = 7.01; EI MS *m/z* (% rel. abund.): 400.25 (M^+, 69.2%).

*4.6.4. (E)-4-(4-oxo-4H-chromen-2-yl)-N′-(2,5-dihydroxybenzylidene)benzohydrazide (**8**)*

Light orange solid; Yield 74%; m.p. > 320 °C; IR (ATR) cm^{-1}: IR (ATR) cm^{-1}: 3244, 3164, 3029, 1647, 1580, 1545, 1487, 1272, 1256, 1141, 747; ^1H NMR (500 MHz, DMSO-*d6*): δ 6.73–6.78 (m, 2H), 6.91 (t, *J* = 7.0 Hz, 1H), 6.97–6.99 (m, 2H), 7.20 (t, *J* = 8.5 Hz, 1H), 7.37 (s, 1H), 7.75 (d, *J* = 7.5 Hz, 1H), 8.00–8.05 (m, 4H), 8.60 (s, 1H), 9.04 (s, 1H), 10.48 (s, 1H), 12.04 (s, 1H); ^{13}C NMR (125 MHz, DMSO-*d6*): δ 105.9, 116.4, 118.1, 118.2, 121.6, 122.0, 125.0, 125.2, 125.4, 125.4, 126.2, 126.9, 126.9, 133.9, 137.1, 138.7, 149.6, 151.2, 152.7, 156.2, 163.4, 164.3, 178.1; Anal. Calcd for $C_{23}H_{16}N_2O_5$: C = 69.00, H = 4.03, N = 7.00; Found: C = 68.69, H = 4.04, N = 6.99; EI MS *m/z* (% rel. abund.): 400.15 (M^+, 71.5%).

*4.6.5. (E)-4-(4-oxo-4H-chromen-2-yl)-N′-(3,4-dihydroxybenzylidene)benzohydrazide (**9**)*

Yellowish white solid; Yield 92%; m.p. 293–295 °C; IR (ATR) cm^{-1}: IR (ATR) cm^{-1}: 3381, 3062, 2898, 1613, 1590, 1558, 1470, 1445, 1277, 1180, 752; ^1H NMR (500 MHz, DMSO-*d6*): δ 6.79 (d, *J* = 8.0 Hz, 1H), 6.91–6.98 (m, 4H), 7.19 (t, *J* = 7.5 Hz, 1H), 7.35 (s, 1H), 7.75 (d, *J* = 7.0 Hz, 1H), 7.76 (s, 1H), 7.99 (m, 4H), 8.29 (s, 1H), 10.23 (s, 1H), 11.59 (s, 1H); ^{13}C NMR (125 MHz, DMSO-*d6*): δ 105.96, 115.90, 116.62, 118.24, 121.06, 125.0, 125.2, 125.44, 125.4, 126.9, 127.9, 127.9, 133.9, 137.1, 138.7, 145.5, 148.1, 148.6, 149.6, 156.2, 163.4, 164.3, 178.9; Anal. Calcd for $C_{23}H_{16}N_2O_5$: C = 69.00, H = 4.03, N = 7.00, Found: C = 69.01, H = 4.02, N = 6.99; EI MS *m/z* (% rel. abund.): 400.27 (M^+, 76.8%).

*4.6.6. (E)-4-(4-oxo-4H-chromen-2-yl)-N′-(2-hydroxybenzylidene)benzohydrazide (**10**)*

White solid; Yield 76%; m.p. 305–306 °C; IR (ATR) cm^{-1}: 3329, 3210, 3021, 1636, 1606, 1537, 1488, 1348, 1259, 1183, 1115, 746; ^1H NMR (500 MHz, DMSO-*d6*): δ 6.91–6.99 (m, 4H), 7.20 (t, *J* = 7.5 Hz, 1H), 7.31 (t, *J* = 8.0 Hz, 1H), 7.37 (s, 1H), 7.56 (d, *J* = 7.5 Hz, 1H), 7.75 (d, *J* = 7.0 Hz, 1H), 8.01–8.06 (m, 4H), 8.67 (s, 1H), 10.28 (s, 1H), 11.32 (s, 1H); ^{13}C NMR (125 MHz, DMSO-*d6*): δ 105.9, 117.3, 118.2, 120.3, 121.1, 125.0, 125.2, 125.4, 125.4, 126.2, 126.9, 126.9, 128.5, 129.7, 133.9, 137.1, 138.7, 151.0, 156.2, 158.3, 163.6, 164.6, 178.1; Anal. Calcd for $C_{23}H_{16}N_2O_4$: C = 71.87, H = 4.20, N = 7.29, Found: C = 71.88, H = 4.22, N = 7.30; EI MS *m/z* (% rel. abund.): 384.32 (M^+, 67.4%).

*4.6.7. (E)-4-(4-oxo-4H-chromen-2-yl)-N′-(3-hydroxybenzylidene)benzohydrazide (**11**)*

Light red solid; Yield 83%; m.p. 299–301 °C; IR (ATR) cm-1: 3385, 3212, 3021, 1626, 1606, 1495, 1466, 1259, 1166, 756; ^1H NMR (500 MHz, DMSO-*d6*): δ 6.84 (d, *J* = 8.0 Hz, 1H), 6.92 (t, *J* = 7.5 Hz, 1H), 6.97 (d, *J* = 8.0 Hz, 1H), 7.12 (d, *J* = 7.5 Hz, 1H), 7.20–7.23 (m, 2H), 7.26 (t, *J* = 7.5 Hz, 1H), 7.75 (s, 1H), 8.01 (m, 5H), 8.39 (s, 1H), 9.67 (s, 1H), 11.85 (s, 1H); ^{13}C NMR (125 MHz, DMSO-*d6*): δ 105.95, 117.32, 118.20, 119.35, 120.08, 125.03, 125.21, 125.4, 125.4, 126.2, 126.9, 126.9, 130.6, 133.9, 136.8, 137.2, 138.7, 148.7, 156.2, 156.7, 163.4, 164.3, 178.1; Anal. Calcd for $C_{23}H_{16}N_2O_4$: C = 71.87, H = 4.20, N = 7.29; Found: C = 71.85, H = 4.22, N = 7.28; EI MS *m/z* (% rel. abund.): 384.13 (M^+, 69.2%);

*4.6.8. (E)-4-(4-oxo-4H-chromen-2-yl)-N′-(4-hydroxybenzylidene)benzohydrazide (**12**)*

Brown solid; Yield 85%; m.p. 292–294 °C; IR (ATR) cm^{-1}: 3429, 3254, 3062, 1607, 1587, 1507, 1467, 1275, 1236, 1180, 755; ^1H NMR (500 MHz, DMSO-*d6*): δ 6.85 (d, *J* = 8.0 Hz, 1H), 6.91 (t, *J* = 7.5 Hz, 1H), 6.97 (d, *J* = 8.0 Hz, 1H), 7.20 (t, *J* = 7.5 Hz, 1H), 7.40 (s, 1H), 7.58 (d, *J* = 8.5 Hz, 2H), 7.75 (s, 1H), 8.00 (m, 5H), 8.38 (s, 1H), 9.98 (s, 1H), 11.70 (s, 1H); ^{13}C NMR (125 MHz, DMSO-*d6*): δ 105.9, 115.6, 115.6, 118.2, 124.3, 124.8, 125.4, 125.4, 125.9, 126.3, 126.8, 126.8, 129.7, 133.8, 137.1, 137.1, 138.6, 149.3, 156.3, 158.4, 163.4, 164.2, 178.0; Anal. Calcd for $C_{23}H_{16}N_2O_4$: C = 71.87, H = 4.20, N = 7.29, Found: C = 71.88, H = 4.21, N = 7.27; EI MS *m/z* (% rel. abund.): 384.18 (M^+, 61.5%).

*4.6.9. (E)-N′-(2-hydroxy-4-methoxybenzylidene)-4-(4-oxo-4H-chromen-2-yl)benzohydrazide (**13**)*

Dark yellow solid; Yield 94%; m.p. 311–312 °C; IR (ATR) cm^{-1}: 3347, 3182, 3075, 2838, 1633, 1603, 1489, 1465, 1260, 1184, 750; ^1H NMR (500 MHz, DMSO-*d6*): δ 3.79 (s, 3H), 6.52 (s, 1H), 6.54 (d, *J* = 8.5 Hz, 1H), 6.92 (t, *J* = 7.5 Hz, 1H), 6.97 (d, *J* = 8.0 Hz, 1H), 7.20 (t, *J* = 8.0 Hz, 1H), 7.44 (d, *J* = 8.5, 1H), 7.75 (s, 1H), 8.02 (m, 5H), 8.58 (s, 1H), 11.65 (s, 1H), 12.04 (s, 1H); ^{13}C NMR (125 MHz, DMSO-*d6*): δ 56.3, 105.9, 107.2, 113.9, 118.2, 124.9, 125.2, 125.4, 125.4, 126.2, 126.9, 126.9, 130.8, 133.9, 137.1, 138.7, 151.0, 156.0, 156.2, 161.2, 162.0, 163.4, 164.3, 178.1; Anal. Calcd for $C_{24}H_{18}N_2O_5$: C = 69.56, H = 4.38, N = 6.76, Found: 69.57, H = 4.39, N = 6.74; EI MS *m/z* (% rel. abund.): 414.03 (M^+, 86.9%).

*4.6.10. (E)-N′-(3-hydroxy-4-methoxybenzylidene)-4-(4-oxo-4H-chromen-2-yl)benzohydrazide (**14**)*

Dark orange solid; Yield 87%; m.p. 293–295 °C; IR (ATR) cm^{-1}: 3389, 3249, 3064, 2843, 1603, 1584, 1561, 1520, 1470, 1440, 1276, 1246, 1171, 752; ^1H NMR (500 MHz, DMSO-*d6*): δ 3.82 (s, 3H), 6.91 (t, *J* = 7.5 Hz, 1H), 6.97 (t, *J* = 8.0 Hz, 2H), 7.08 (d, *J* = 8.0 Hz, 1H), 7.20 (t, *J* = 8.0 Hz, 1H), 7.29 (s, 1H), 7.39 (s, 1H), 7.76 (s, 1H), 8.00 (s, 4H), 8.33 (s, 1H), 9.35 (s, 1H), 11.72 (s, 1H); ^{13}C NMR (125 MHz, DMSO-*d6*): δ 56.4, 105.8, 115.0, 115.2, 118.2, 120.3, 125.0, 125.3, 125.5, 125.5, 126.2, 126.8, 126.8, 129.5, 133.8, 137.2, 138.6, 146.6, 148.5, 149.7, 156.8, 163.4, 164.4, 178.8; Anal. Calcd for $C_{24}H_{18}N_2O_5$: C = 69.56, H = 4.38, N = 6.76, Found: C = 69.55, H = 4.39, N = 6.74; EI MS *m/z* (% rel. abund.): 414.24 (M^+, 65.0%).

*4.6.11. (E)-N′-(2-hydroxy-5-methoxybenzylidene)-4-(4-oxo-4H-chromen-2-yl)benzohydrazide (**15**)*

Dark orange solid; Yield 68%; m.p. 305–307 °C; IR (ATR) cm^{-1}:

3143, 2962, 2835, 1642, 1614, 1583, 1490, 1462, 1266, 1164, 756; ^{1}H NMR (500 MHz, DMSO-*d6*): δ 3.75 (s, 3H), 6.87–6.99 (m, 4H), 7.14 (s, 1H), 7.20 (t, *J* = 7.5 Hz, 1H), 7.37 (s, 1H), 7.76 (s, 1H), 8.02 (m, 4H), 8.66 (s, 1H), 10.71 (s, 1H), 12.02 (s, 1H); ^{13}C NMR (125 MHz, DMSO-*d6*): δ 56.3, 105.9, 112.8, 116.3, 116.5, 118.2, 121.7, 124.9, 125.1, 125.3, 125.3, 126.2, 126.9, 126.9, 133.9, 137.1, 138.7, 149.6, 154.2, 154.4, 156.2, 163.4, 164.3, 178.2; Anal. Calcd for $C_{24}H_{18}N_2O_5$: C = 69.56, H = 4.38, N = 6.76, Found: C = 69.57, H = 4.36, N = 6.78; EI MS *m/z* (% rel. abund.): 414.19 (M^+, 72.5%).

4.6.12. (E)-N′-(3,5-dimethoxybenzylidene)-4-(4-oxo-4H-chromen-2-yl)benzohydrazide (**16**)

Light orange solid; Yield 71%; m.p. 232–234 °C; IR (ATR) cm^{-1}: 3394, 3296, 3002, 2837, 1684, 1652, 1585, 1462, 1266, 1205, 1157, 736; ^{1}H NMR (500 MHz, DMSO-*d6*): δ 3.86 (s, 6H), 6.57 (s, 1H), 6.95 (m, 2H), 7.09 (s, 2H), 7.21 (m, 2H), 7.74 (d, *J* = 7.5 Hz, 1H), 8.00 (d, *J* = 8.0 Hz, 2H), 8.06 (d, *J* = 8.0 Hz, 2H), 8.30 (s, 1H), 11.97 (s, 1H); ^{13}C NMR (125 MHz, DMSO-*d6*): δ 56.2, 56.2, 98.5, 105.4, 105.4, 105.9, 118.4, 124.9, 125.2, 125.5, 125.5, 126.2, 126.9, 126.9, 133.9, 137.1, 138.2, 138.7, 147.9, 156.3, 161.2, 161.2, 163.4, 164.3, 178.3; Anal. Calcd for $C_{25}H_{20}N_2O_5$: C = 70.09, H = 4.71, N = 6.54, Found: C = 70.07, H = 4.70, N = 6.55; EI MS *m/z* (% rel. abund.): 428.35 (M^+, 54.1%).

4.6.13. (E)-N′-(3-bromo-4-hydroxybenzylidene)-4-(4-oxo-4H-chromen-2-yl)benzohydrazide (**17**)

Brown solid; Yield 79%; m.p. 254–255 °C; IR (ATR) cm^{-1}: 3352, 3140, 3054, 2897, 1650, 1591, 1496, 1282, 1205, 750; ^{1}H NMR (500 MHz, DMSO-*d6*): δ 6.91 (t, *J* = 7.5 Hz, 1H), 6.99 (s, 1H), 7.03 (d, *J* = 8.0 Hz, 1H), 7.20 (t, *J* = 8.5 Hz, 1H), 7.58 (d, *J* = 8.5 Hz, 1H), 7.73 (s, 1H), 7.89 (s, 1H), 8.00 (m, 5H), 8.35 (s, 1H), 10.78 (s, 1H), 11.83 (s, 1H); ^{13}C NMR (125 MHz, DMSO-*d6*): δ 105.9, 109.9, 116.3, 118.2, 125.1, 125.4, 125.4, 125.4, 125.7, 126.2, 126.9, 126.9, 128.2, 130.4, 133.9, 137.1, 138.7, 148., 153.7, 156.2, 163.4, 164.3, 178.1; Anal. Calcd for $C_{23}H_{15}BrN_2O_4$: C = 59.63, H = 3.26, N = 6.05, Found: C = 59.64, H = 3.24, N = 6.06; EI MS *m/z* (% rel. abund.): 462.02 (M+, 54.7%).

4.6.14. (E)-N′-(2-methylbenzylidene)-4-(4-oxo-4H-chromen-2-yl) benzohydrazide (**18**)

White solid; Yield 85%; m.p. 225–226 °C; IR (ATR) cm^{-1}: 3433, 3253, 3021, 2361, 1609, 1546, 1466, 1277, 755; ^{1}H NMR (500 MHz, DMSO-*d6*): δ 2.47 (s, 3H), 6.91 (t, *J* = 7.5 Hz, 1H), 6.98 (s, 1H), 7.20 (t, *J* = 7.5 Hz, 1H), 7.27–7.34 (m, 4H), 7.87 (d, *J* = 7.5 Hz, 1H), 8.02 (m, 5H), 8.78 (s, 1H), 11.88 (s, 1H); ^{13}C NMR (125 MHz, DMSO-*d6*): δ 21.1, 105.9, 118.2, 125.1, 125.3, 125.5, 125.5, 126.0, 126.3, 126.6, 126.9, 126.9, 128.2, 130.5, 133.5, 133.8, 135.4, 137.1, 138.6, 145.4, 156.3, 163.5, 164.3, 178.1; Anal. Calcd for $C_{24}H_{18}N_2O_3$: C = 75.38, H = 4.74, N = 7.33, Found: C = 75.39, H = 4.75, N = 7.31; EI MS *m/z* (% rel. abund.): 382.29 (M^+, 70.3%).

4.6.15. (E)-N′-(3-methylbenzylidene)-4-(4-oxo-4H-chromen-2-yl) benzohydrazide (**19**)

White solid; Yield 93%; m.p. 210–211 °C; IR (ATR) cm^{-1}: 3406, 3193, 3023, 1625, 1557, 1309, 1256, 747; ^{1}H NMR (500 MHz, DMSO-*d6*): δ 2.37 (s, 3H), 6.91 (t, *J* = 7.0 Hz, 1H), 6.98 (d, *J* = 7.5 Hz, 1H), 7.20 (t, *J* = 8.0 Hz, 1H), 7.27(d, *J* = 7.5 Hz, 1H), 7.35 (t, *J* = 7.5 Hz, 1H), 7.45 (s, 1H), 7.53 (d, *J* = 7.5 Hz, 1H), 7.59 (s, 1H), 7.75 (s, 1H), 8.01 (m, 4H), 8.45 (s, 1H), 11.89 (s, 1H); ^{13}C NMR (125 MHz, DMSO-*d6*): δ 21.4, 105.9, 118.2, 123.5, 124.8, 125.2, 125.5, 125.5, 126.0, 126.8, 126.8, 128.2, 128.6, 129.7, 133.8, 136.6, 137.2, 137.9, 138.8, 148.7, 156.2, 163.4, 164.3, 178.3; Anal. Calcd for $C_{24}H_{18}N_2O_3$: C = 75.38, H = 4.74, N = 7.33, Found: C = 75.39, H = 4.73, N = 7.31; EI MS *m/z* (% rel. abund.): 382.12 (M^+, 61.7%).

4.6.16. (E)-N′-(4-methylbenzylidene)-4-(4-oxo-4H-chromen-2-yl) benzohydrazide (**20**)

Light yellow solid; Yield 74%; m.p. 232–234 °C; IR (ATR) cm^{-1}: 3422, 3382, 3242, 3164, 1609, 1464, 1270, 749; ^{1}H NMR (MeOD-d_4, 500 MHz): δ 2.41 (s, 3H), 6.94–6.98 (m, 2H), 7.21–7.24 (m, 2H), 7.29 (d, *J* = 8.0 Hz, 2H), 7.75–7.77 (m, 3H), 7.99 (d, *J* = 7.5 Hz, 2H), 8.06 (d, *J* = 7.5 Hz, 2H), 8.36 (s, 1H), 12.27 (s, 1H); ^{13}C-HMR (125 MHz, DMSO-*d6*): δ 21.15, 105.9, 118.2, 125.0, 118.2, 125.0, 125.3, 125.3, 125.8, 126.1, 126.8, 126.8, 127.3, 129.2, 131.8, 133.9, 137.2, 138.2, 138.7, 149.4, 156.3, 163.5, 164.5, 178.0; Anal. Calcd for $C_{24}H_{18}N_2O_3$: C = 75.38, H = 4.74, N = 7.33, Found: C = 75.39, H = 4.76, N = 7.31; EI MS *m/z* (% rel. abund.): 382.07 (M^+, 62.5%).

4.6.17. (E)-N′-(2-chlorobenzylidene)-4-(4-oxo-4H-chromen-2-yl) benzohydrazide (**21**)

White solid; Yield 78%; m.p. 294–296 °C; IR (ATR) cm^{-1}: 3432, 3183, 3065, 1613, 1589, 1543, 1467, 1280, 757; ^{1}H NMR (500 MHz, DMSO-*d6*): δ 1H NMR (MeOD-d4, 500 MHz): δ 6.94–6.98 (m, 2H), 7.21–7.25 (m, 2H), 7.42–7.46 (m, 2H), 7.48 (d, *J* = 8.0 Hz, 1H), 7.75 (dd, *J* = 7.5 Hz, 1.5 Hz, 1H), 8.00 (d, *J* = 7.0 Hz, 2H), 8.08 (d, *J* = 7.5 Hz, 2H), 8.31 (dd, *J* = 7.5 Hz, 1.5 Hz, 1H), 8.91 (s, 1H), 12.23 (s, 1H); ^{13}C NMR (125 MHz, DMSO-*d6*): δ 105.9, 118.2, 125.0, 125.2, 125.4, 125.4, 126.5, 126.9, 126.9, 127.3, 127.5, 128.6, 130.9, 131.3, 132.7, 133.9, 137.1, 138.7, 149.8, 156.2, 163.2, 164.3, 178.1; Anal. Calcd for $C_{23}H_{15}ClN_2O_3$: C = 68.58, H = 3.75, N = 6.95, Found: C = 68.59, H = 3.76, N = 6.93; EI MS *m/z* (% rel. abund.): 402.08 (M+, 74.2%), 404.08 (M+2, 13.8%).

4.6.18. (E)-N′-(3-chlorobenzylidene)-4-(4-oxo-4H-chromen-2-yl) benzohydrazide (**22**)

Light yellow solid; Yield 69%; m.p. 304–306 °C; IR (ATR) cm^{-1}: 3273, 3120, 2915, 1660, 1542, 1469, 1253, 743; ^{1}H NMR (500 MHz, DMSO-*d6*): δ 6.89 (t, *J* = 7.5 Hz, 1H), 6.96 (d, *J* = 8.0 Hz, 1H), 7.18 (t, *J* = 8.0 Hz, 1H), 7.34 (s, 1H), 7.51 (d, *J* = 4.0 Hz, 2H), 7.72–7.75 (m, 2H), 7.81 (s, 1H), 8.02 (s, 4H), 8.47 (s, 1H), 12.06 (s, 1H); ^{13}C NMR (125 MHz, DMSO-*d6*): δ 105.9, 118.2, 124.4, 124.8, 125.2, 125.4, 125.4, 126.2, 126.9, 126.9, 127.6, 128.0, 130.2, 133.7, 134.0, 135.3, 137.1, 138.7, 148.6, 156.2, 163.4, 164.3, 178.2; Anal. Calcd for $C_{23}H_{15}ClN_2O_3$: C = 68.58, H = 3.75, N = 6.95, Found: C = 68.57, H = 3.77, N, 6.97; EI MS *m/z* (% rel. abund.): 402.08 (M+, 35.4%), 404.36 (M+2, 13.8%).

4.6.19. (E)-N′-(4-chlorobenzylidene)-4-(4-oxo-4H-chromen-2-yl) benzohydrazide (**23**)

Yellow solid; Yield 91%; m.p. 295–297 °C; IR (ATR) cm^{-1}: 3427, 3126, 2947, 1608, 1589, 1466, 1273, 752; ^{1}H NMR (MeOD-d_4, 500 MHz): δ 6.94–6.98 (m, 2H), 7.21 (td, *J* = 8.5 Hz, 1.0 Hz, 1H), 7.24 (s, 1H), 7.48 (d, *J* = 8.5 Hz, 2H), 7.75 (dd, *J* = 7.5 Hz, 1.5 Hz, 1H), 7.87 (d, *J* = 8.5 Hz, 2H), 8.00 (d, *J* = 7.5 Hz, 2H), 8.02 (d, *J* = 8.0 Hz, 2H), 8.38 (s, 1H), 12.03 (s, 1H); ^{13}C NMR (125 MHz, DMSO-*d6*): δ 105.9, 118.4, 125.1, 125.4, 125.4, 125.8, 126.3, 126.8, 126.8, 129.0, 129.0, 129.4, 129.4, 132.3, 134.1, 135.1, 137.1, 138.7, 149.4, 156.3, 163.3, 164.3, 178.3. Anal. Calcd for $C_{23}H_{15}ClN_2O_3$: C = 68.58, H = 3.75, N = 6.95, Found: C = 68.59, H = 3.74, N = 6.94; EI MS *m/z* (% rel. abund.): 402.08 (M+, 64.7%), 404.21 (M+2, 13.8%).

4.6.20. (E)-N′-(2-nitrobenzylidene)-4-(4-oxo-4H-chromen-2-yl) benzohydrazide (**24**)

Yellow solid; Yield 65%; m.p. 305–306 °C; IR (ATR) cm^{-1}: 3431, 3255, 3153, 3024, 1623, 1543, 1519, 1468, 1274, 755; ^{1}H NMR (MeOD-d_4, 500 MHz): δ 6.91 (t, *J* = 7.5 Hz, 1H), 6.98 (d, *J* = 7.5 Hz, 1H), 7.20 (t, *J* = 7.5 Hz, 1H), 7.37 (s, 1H), 7.69–7.93 (m, 3H), 8.03–8.18 (m, 6H), 8.91 (s, 1H), 12.26 (s, 1H); ^{13}C NMR (125 MHz, DMSO-*d6*): δ 105.91, 118.28, 125.00, 125.1, 125.2, 125.4, 125.4, 126.2, 126.9, 126.9, 128.0, 129.3, 130.4, 132.6, 133.7, 137.1, 138.7, 142.9, 147.9, 156.9, 163.4, 164.3, 178.1; Anal. Calcd for $C_{23}H_{15}N_3O_5$: C = 66.83, H = 3.66, N = 10.17, Found: C = 66.84, H = 3.65, N = 10.19; EI MS *m/z* (% rel.

abund.): 413.07 (M^+, 42.7%).

*4.6.21. (E)-N′-(3-nitrobenzylidene)-4-(4-oxo-4H-chromen-2-yl) benzohydrazide (**25**)*

Light orange solid; Yield 62%; m.p. 312–314 °C; IR (ATR) cm^{-1}: 3312, 3179, 3143, 2886, 1657, 1519, 1469, 1342, 1274, 1145, 732; ^1H NMR (500 MHz, DMSO-*d6*): δ 6.91 (t, *J* = 7.5 Hz, 1H), 6.98 (d, *J* = 8.0 Hz, 1H), 7.20 (t, *J* = 7.5 Hz, 1H), 7.37 (s, 1H), 7.75–7.77 (m, 2H), 8.03 (m, 4H), 8.17 (d, *J* = 6.5 Hz, 1H), 8.27(d, *J* = 7.5 Hz, 1H), 8.57–8.60 (m, 3H), 12.16 (s, 1H); ^{13}C NMR (125 MHz, DMSO-*d6*): δ 105.94, 118.22, 122.37, 124.18, 125.05, 125.24, 125.5, 125.5, 126.2, 126.9, 126.9, 129.9, 132.6, 133.9, 137.1, 137.7, 138.7, 147.41, 148.6, 156.2, 163.4, 164.3, 178.1; Anal. Calcd for $C_{23}H_{15}N_3O_5$: C = 66.83, H = 3.66, N = 10.17, Found: C = 66.84, H = 3.65, N = 10.18; EI MS *m/z* (% rel. abund.): 413.15 (M^+, 52.6%).

*4.6.22. (E -(4-nitrobenzylidene)-4-(4-oxo-4H-chromen-2-yl) benzohydrazide (**26**)*

Dark brown solid; Yield 88%; m.p. 297–299 °C; IR (ATR) cm^{-1}: 3413, 3075, 2833, 1633, 1514, 1466, 1341, 1269, 1113, 756; ^1H NMR (500 MHz, DMSO-*d6*): δ 6.92 (t, *J* = 7.5 Hz, 1H), 6.98 (d, *J* = 8.0 Hz, 1H), 7.20 (t, *J* = 7.5 Hz, 1H), 7.37 (s, 1H), 7.75 (d, *J* = 7.0 Hz, 1H), 8.03 (m, 6H), 8.32–8.33 (m, 2H), 8.59 (s, 1H), 12.22 (s, 1H); ^{13}C NMR (125 MHz, DMSO-*d6*): δ 106.5, 118.2, 124.4, 124.4, 125.0, 125.2, 125.4, 125.4, 125.6, 126.2, 126.9, 126.9, 127.9, 127.9, 133.9, 137.1, 138.7, 148.0, 149.3, 156.2, 163.4, 164.3, 178.1; Anal. Calcd for $C_{23}H_{15}N_3O_5$: C = 66.83, H = 3.66, N = 10.17, Found: C = 66.82, H = 3.67, N = 10.18; EI MS *m/z* (% rel. abund.): 413.19 (M^+, 64.8%).

*4.6.23. (E)-N′-(2-fluorobenzylidene)-4-(4-oxo-4H-chromen-2-yl) benzohydrazide (**27**)*

White solid; Yield 84%; m.p. 257–259 °C; IR (ATR) cm^{-1}: 3434, 3232, 3019, 2861, 1660, 1608, 1519, 1466, 1360, 1272, 1187, 752; ^1H NMR (MeOD-d_4, 500 MHz): δ 6.96–6.98 (m, 2H), 7.19–7.24 (m, 3H), 7.28 (t, *J* = 7.5 Hz, 1H), 7.48 (d, *J* = 8.0 Hz, 1H), 7.74 (dd, *J* = 7.5 Hz, 1.5 Hz, 1H), 8.00 (d, *J* = 8.5 Hz, 2H), 8.07 (d, *J* = 8.5 Hz, 2H), 8.24 (t, *J* = 7.5 Hz, 1H), 8.70 (s, 1H), 12.11 (s, 1H); ^{13}C NMR (125 MHz, DMSO-*d6*): δ 105.9, 117.4, 118.3, 124.6, 125.1, 125.4, 125.4, 125.6, 125.8, 126.3, 126.9, 126.9, 129.4, 130.9, 133.9, 137.1, 138.7, 149.3, 156.1, 159.3 (d, *J* = 282.5 Hz), 163.4, 164.3, 178.3; Anal. Calcd for $C_{23}H_{15}FN_2O_3$: C = 71.50, H = 3.91, F = 4.92, N = 7.25, Found: C = 71.51, H = 3.89, F = 4.91, N = 7.26; EI MS *m/z* (% rel. abund.): 386.06 (M^+, 72.6%).

*4.6.24. (E)-N′-(3-fluorobenzylidene)-4-(4-oxo-4H-chromen-2-yl) benzohydrazide (**28**)*

White solid; Yield 78%; m.p. 254–256 °C; IR (ATR) cm-1: 3119, 3026, 2828, 1658, 1539, 1449, 1269, 745; ^1H NMR (MeOD-d_4, 500 MHz): δ 6.94–6.98 (m, 2H), 7.18–7.24 (m, 3H), 7.46 (d, *J* = 8.0 Hz, 1H), 7.62 (d, *J* = 7.5 Hz, 1H), 7.72–7.76 (m, 2H), 8.00 (d, *J* = 7.5 Hz, 2H), 8.06 (d, *J* = 8.0 Hz, 2H), 8.38 (s, 1H), 12.20 (s, 1H); ^{13}C NMR (125 MHz, DMSO-*d6*): δ 105.8, 114.4, 117.1, 118.4, 121.8, 124.7, 125.2, 125.7, 125.7, 126.2, 126.9, 126.9, 129.9, 133.9, 137.1, 138.2, 138.7, 148.6, 156.2, 161.6 (d, *J* = 193.75 Hz), 163.7, 164.4, 178.1; Anal. Calcd for $C_{23}H_{15}FN_2O_3$: C = 71.50, H = 3.91, N = 7.25. Found: C = 71.51, H = 3.93, F = 4.91, N = 7.24; EI MS *m/z* (% rel. abund.): 386.11 (M^+, 62.7%).

*4.6.25. (E)-N′-(4-fluorobenzylidene)-4-(4-oxo-4H-chromen-2-yl) benzohydrazide (**29**)*

Light yellow solid; Yield 95%; m.p. 252–254 °C; IR (ATR) cm-1: 3421, 3282, 3061, 2947, 1633, 1609, 1505, 1467, 1233, 752; ^1H NMR (500 MHz, DMSO-*d6*): δ 6.92 (t, *J* = 7.0 Hz, 1H), 6.98 (d, *J* = 8.0 Hz, 1H), 7.20 (t, *J* = 7.5 Hz, 1H), 7.30–7.36 (m, 3H), 7.75–7.82(m, 3H), 8.02(m, 4H), 8.49(s, 1H), 11.92(s, 1H); ^{13}C NMR (125 MHz, DMSO-*d6*): δ 105.9, 115.3, 115.3, 115.6, 118.2, 124.6, 125.3, 125.7, 125.7, 126.2, 126.9, 126.9, 130.3, 130.8, 130.8, 133.8, 137.1, 138.7, 149.3, 156.2, 160.3 (d, *J* = 245.00 Hz), 163.3, 164.3, 178.2; Anal. Calcd for $C_{23}H_{15}FN_2O_3$: C = 71.50, H = 3.91, N = 7.25, Found: C = 71.49, H = 3.93, N = 7.26; EI MS *m/z* (% rel. abund.): 386.41 (M^+, 47.1%).

*4.6.26. (E)-N′-(3-methoxybenzylidene)-4-(4-oxo-4H-chromen-2-yl)benzohydrazide (**30**)*

Light brown solid; Yield 91%; m.p. 231–233 °C; IR (ATR) cm-1: 3539, 3252, 3051, 2835, 1640, 1564, 1469, 1253, 1141, 747; ^1H NMR (MeOD-d_4, 500 MHz): δ 3.90 (s, 3H), 6.94–6.98 (m, 2H), 7.02 (d, *J* = 8.0 Hz, 1H), 7.21–7.25 (m, 2H), 7.33–7.39 (m, 2H), 7.62 (s, 1H), 7.75 (d, *J* = 6.5 Hz, 1H), 8.00 (d, *J* = 7.0 Hz, 2H), 8.07 (d, *J* = 7.5 Hz, 2H), 8.36 (s, 1H), 12.08 (s, 1H); ^{13}C NMR (125 MHz, DMSO-*d6*): δ 56.2, 105.9, 112.2, 114.8, 118.2, 121.2, 124.9, 125.2, 125.4, 125.4, 126.2, 126.9, 126.9, 129.2, 133.9, 136.9, 137.1, 138.7, 148.6, 156.3, 160.2, 163.2, 164.2, 178.3; Anal. Calcd for $C_{24}H_{18}N_2O_4$: C = 72.35; H = 4.55; N = 7.03, Found: C = 72.33; H = 4.56; N = 7.01; EI MS *m/z* (% rel. abund.): 398.26 (M^+, 51.7%).

*4.6.27. (E)-N′-(4-methoxybenzylidene)-4-(4-oxo-4H-chromen-2-yl)benzohydrazide (**31**)*

Yellow solid; Yield 89%; m.p. 237–239 °C; IR (ATR) cm-1: 3424, 3269, 3065, 2843, 1610, 1507, 1466, 1356, 1244, 755; ^1H NMR (500 MHz, DMSO-*d6*): δ 3.83 (s, 3H), 6.92 (t, *J* = 7.0 Hz, 1H), 6.97 (d, *J* = 8.0 Hz, 1H), 7.04 (d, *J* = 8.5 Hz, 2H), 7.20 (t, *J* = 7.0 Hz, 1H), 7.36 (s, 1H), 7.70–7.77 (m, 3H), 8.00 (s, 4H), 8.44 (s, 1H), 11.77 (s, 1H); ^{13}C NMR (125 MHz, DMSO-*d6*): δ 56.0, 105.9, 114.3, 114.3, 118.2, 125.0, 125.2, 125.4, 125.4, 126.2, 126.6, 127.0, 127.0, 129.1, 129.1, 133.9, 137.1, 138.7, 149.3, 156.2, 160.1, 163.2, 164.6, 178.3. Anal. Calcd for $C_{24}H_{18}N_2O_4$: C = 72.35, H = 4.55, N = 7.03, Found: C = 72.36, H = 4.53, N = 7.02; EI MS *m/z* (% rel. abund.): 398.17 (M^+, 69.4%).

*4.6.28. (E)-4-(4-oxo-4H-chromen-2-yl)-N′-(pyridin-2-ylmethylene)benzohydrazide (**32**)*

Orange solid; Yield 81%; m.p. 170–172 °C; IR (ATR) cm-1: 3395, 3170, 3058, 2849, 1643, 1564, 1465, 1255, 734; ^1H NMR (MeOD-d_4, 500 MHz): δ 6.95–6.98 (m, 2H), 7.21–7.26 (m, 2H), 7.46 (d, *J* = 5.0 Hz, 1H), 7.75 (d, *J* = 8.0 Hz, 1H), 7.93 (t, *J* = 7.5 Hz, 1H), 8.01–8.02 (m, 2H), 8.07–8.13 (m, 3H), 8.34 (d, *J* = 7.5 Hz, 1H), 8.45 (s, 1H), 11.78 (s, 1H); ^{13}C NMR (125 MHz, DMSO-*d6*): δ 105.9, 118.2, 119.0, 123.0, 125.0, 125.2, 125.4, 125.4, 126.3, 126.9, 126.9, 133.9, 137.1, 137.6, 138.7, 146.1, 147.9, 154.6, 156.2, 163.2, 164.5, 178.0. Anal. Calcd for $C_{22}H_{15}N_3O_3$: C = 71.54, H = 4.09, N = 11.38, Found: C = 71.55, H = 4.10, N = 11.39; EI MS *m/z* (% rel. abund.): 369.21 (M^+, 47.0%).

*4.6.29. (E)-4-(4-oxo-4H-chromen-2-yl)-N′-(pyridin-3-ylmethylene)benzohydrazide (**33**)*

Orange solid; Yield 79%; m.p. 210–212 °C; IR (ATR) cm-1: 3417, 3037, 2837, 1641, 1556, 1467, 1280, 755; ^1H NMR (MeOD-d_4, 500 MHz): δ 6.96 (m, 2H), 7.21–7.24 (m, 2H), 7.55 (d, *J* = 5.0 Hz, 1H), 7.75 (d, *J* = 5.5 Hz, 1H), 8.00–8.07 (m, 4H), 8.43–8.45 (m, 2H), 8.61 (d, *J* = 3.5 Hz, 1H), 8.95 (s, 1H), 12.21 (s, 1H); ^{13}C NMR (125 MHz, DMSO-*d6*): δ 105.9, 118.2, 124.41, 125.0, 125.2, 125.4, 125.4, 126.2, 126.9, 126.9, 133.8, 134.6, 135.6, 137.1, 138.7, 145.5, 146.3, 149.8, 156.2, 163.4, 164.2, 178.1; Anal. Calcd for $C_{22}H_{15}N_3O_3$: C = 71.54, H = 4.09, N = 11.38, Found: C = 71.53, H = 4.08, N = 11.37; EI MS *m/z* (% rel. abund.): 369.15 (M^+, 67.0%).

*4.6.30. (E)-4-(4-oxo-4H-chromen-2-yl)-N′-(pyridin-4-ylmethylene)benzohydrazide (**34**)*

Dark red solid; Yield 76%; m.p. 198–200 °C; IR (ATR) cm-1: 3289, 3172, 2850, 1657, 1544, 1466, 1262, 1113, 754; ^1H NMR (MeOD-d_4, 500 MHz): δ 6.94–6.98 (m, 2H), 7.21 (t, *J* = 7.5 Hz, 1H), 7.25 (s, 1H),

7.74 (dd, J = 8.0 Hz, 1.5 Hz, 1H), 7.88 (d, J = 5.0 Hz, 2H), 8.01 (d, J = 8.5 Hz, 2H), 8.08 (d, J = 8.0 Hz, 2H), 8.39 (s, 1H), 8.64 (d, J = 5.5 Hz, 2H), 12.76 (s, 1H); ^{13}C NMR (125 MHz, DMSO-*d6*): δ 105.9, 118.2, 122.3, 122.3, 125.0, 125.28, 125.4, 125.4, 126.2, 126.9, 126.9, 133.9, 137.1, 138.7, 140.7, 149.3, 150.0, 150.0, 156.2, 163.4, 164.3, 178.1. Anal. Calcd for $C_{22}H_{15}N_3O_3$: C = 71.54, H = 4.09, N = 11.38, Found: C = 71.56, H = 4.11, N = 11.36; EI MS *m/z* (% rel. abund.): 369.07 (M+, 64.5%).

4.7. α-Glucosidase inhibition assay

The α-glucosidase inhibition assay had been carried out using baker's yeast α-glucosidase (EC 3.2.1.20) and *p*-nitrophenyl-α-D-glucopyranoside [49]. The samples (5 μg/mL) were prepared by dissolving the compounds **1**–**35** in DMSO. Test samples (10 μL) which had been prepared were reconstituted in 100 μL of phosphate buffer (100 mM) at pH 6.8 in 96-well micro-plate and incubated with 50 μL of baker's yeast α-glucosidase for 5 min before 50 μL of *p*-nitrophenyl-α-D-glucopyranoside (5 mM) was added. After incubating for 5 min, the absorbance was measured at 405 nm using SpectraMax plus384 (Molecular Devices Corporation, Sunnyvale, CA, USA). Blank in which the substrate was changed with 50 μL of buffer were analyzed to accurately determine the background absorbance. Control sample was prepared to contain 10 μL DMSO instead of test samples. Percentage of enzyme inhibition was measured using the following formula.

$$\%\ \text{inhibition} = [(A - B)/A] \times 100$$

[A] represents absorbance of control samples, and [B] corresponding to absorbance in presence of test samples.

4.8. In vitro HDAC inhibition assay

This assay had been performed in accordance with method in Li et al. (2014) [50]. In this assay, 10 μL of enzyme solution was mixed with 50 μL of tested compound at various concentrations. The mixture was incubated at 37 °C for 5 min prior to addition of 40 μL fluorogenic substrate Boc-Lys (acetyl)-AMC. After further incubation at 37 °C for 30 min, the reaction was stopped by adding 100 μL of trypsin and TSA. Fluorescence intensity was measured after 20 min using a microplate reader at excitation and emission wavelengths of 390 and 460 nm, respectively.

4.9. Cytotoxicity

The Neutral Red cytotoxicity assay is based on the initial protocol described by Borenfreund et al. (1998) [51] with some modifications. Briefly, the cells (1×10^4/well) were seeded in 96-well microtiter plates (Nunc) and allowed to grow for 24 h before treatment. After 24 h of incubation, the cells were treated with six different concentrations (0.1–100 μg/mL) of test compounds, in three replicates. The plates were incubated for 72 h at 37 °C in a 5% CO_2 incubator. A stock solution was obtained by dissolving the test compounds in DMSO. Further dilution to different tested concentrations were then carried out ensuring that the final concentration of DMSO in the test and control wells was not in excess of 1% (v/v). No effect due to the DMSO was observed. Doxorubicin was used as the positive control. The well containing untreated cells was the negative control. At the end of the incubation period, the media were replaced with medium containing 50 μg/mL of Neutral Red. The plates were incubated for another 3 h to allow for uptake of the vital dye into the lysosomes of viable and injured cells. After the incubation period, the media were removed and cells were washed with the neutral red washing solution. The dye was eluted from the cells by adding 200 μL of Neutral Red resorb solution and incubated for 30 min at room temperature with rapid agitation on a microtiter plate shaker. Dye absorbance was measured at 540 nm using a spectrophotometer ELISA plate reader.

4.10. 2D QSAR

Training set and test set compounds were being selected using "Cluster Ligands" protocol in Discovery Studio DS 2.5 software (Discovery Studio 2.5, Accelrys, Co. Ltd). Another module, "Calculate Molecular Properties", was used to calculate the 2D molecular properties as well as energies of highest occupied and lowest unoccupied molecular orbitals (HOMO and LUMO) of the training set compounds. All semi-empirical calculation and density functional theory was carried out using software package VAMP and DMol3 in Discovery Studio 2.5. Different 2D descriptors such as AlogP, molecular properties (molecular weight), molecular property counts (Num_aromatic Rings, Num_-H_Acceptors, Num_H_Donors, Num_Rings and Num_Rotatable Bonds) and surface area and volume (Molecular_Fractional Polar Surface Area), were utilized in our model. The model was validated using test set correlation and Leave-one-out (LOO) cross validation.

4.11. Docking studies

The structure of all compounds were prepared using Chem3D by CambridgeSoft. The geometry and energy of the structures were being optimized using Steepest-Descent and Polak-Ribiere algorithm in HyperChem. AutoDock 4.2 [52] was used to identify the binding modes of flavone derivatives (**5**–**34**) responsible for the activity. Genetic Algorithm (GA) with default settings was employed for the studies. Protein sequence for Baker's yeast α-glucosidase (MAL12) was obtained from uniprot (http://www.uniprot.org). Homology model for *S. cerevisiae* α-glucosidase was built using crystal structure of α-D-glucose bound isomaltase from *S. cerevisiae* (PDB ID: 3A4A) which shares 72% identical and 85% similar sequence with α-glucosidase. Sequence alignment and homology modeling were performed using Swiss-Model, which is a fully automated homology modeling pipeline SWISS-MODEL, managed by Swiss Institute of Bioinformatics [53–55]. The docking results had been visualized using Discovery Studio visualizer 3.5 [56] and PyMol [57]. The homology model was being evaluated by using PROCHECK [58,59].

Acknowledgment

The authors would like to acknowledge Universiti Teknologi MARA for the financial support through research grant, UiTM 100-RMI/MOA 16/6/2 (1/2013). The first author would like to thank UiTM and Ministry of Higher Education Malaysia for the financial funding through Dana Kecemerlangan Pendidikan UiTM and MyBrain15 scholarship.

Appendix A. Supplementary data

Supplementary data related to this article can be found at http://dx.doi.org/10.1016/j.ejmech.2015.10.017.

References

[1] Y.-G. Chen, P. Li, P. Li, R. Yan, X.-Q. Zhang, Y. Wang, X.-T. Zhang, W.-C. Ye, Q.-W. Zhang, α-Glucosidase inhibitory effect and simultaneous quantification of three major flavonoid glycosides in Microctis folium, Molecules 18 (2013) 4221–4232.
[2] G. Danaei, M.M. Finucane, Y. Lu, G.M. Singh, M.J. Cowan, C.J. Paciorek, J.K. Lin, F. Farzadfar, Y.-H. Khang, G.A. Stevens, M. Rao, M.K. Ali, L.M. Riley,

C.A. Robinson, M. Ezzati, National, regional, and global trends in fasting plasma glucose and diabetes prevalence since 1980: systematic analysis of health examination surveys and epidemiological studies with 370 country-years and 2 7 million participants, Lancet 378 (9785) (2011) 31–40.
[3] N. Asano, Glycosidase inhibitors: update and perspectives on practical use, Glycobiology 13 (2003) 93R–104R.
[4] M.J. Humphries, K. Matsumoto, S.L. White, K. Olden, Inhibition of experimental metastasis by castanospermine in mice: blockage of two distinct stages of tumor colonization by oligosaccharide processing inhibitors, Cancer Res. 46 (1986) 5215–5222.
[5] H. Park, K.Y. Hwang, K.H. Oh, Y.H. Kim, J.Y. Lee, K. Kim, Discovery of novel α-glucosidase inhibitors based on the virtual screening with the homology-modeled protein structure, Bioorg. Med. Chem. 16 (2008) 284–292.
[6] S.J. Storr, L. Royle, C.J. Chapman, U.M.A. Hamid, J.F. Robertson, A. Murray, R.A. Dwek, P.M. Rudd, The O-linked glycosylation of secretory/shed MUC1 from an advanced breast cancer patient's serum, Glycobiology 18 (2008) 456–462.
[7] D.P. Gamblin, E.M. Scanlan, B.G. Davis, Glycoprotein synthesis: an update, Chem. Rev. 109 (2008) 131–163.
[8] H. Park, K.Y. Hwang, Y.H. Kim, K.H. Oh, J.Y. Lee, K. Kim, Discovery and biological evaluation of novel α-glucosidase inhibitors with in vivo antidiabetic effect, Bioorg. Med. Chem. Lett. 18 (2008) 3711–3715.
[9] A.J. Rawlings, H. Lomas, A.W. Pilling, M.J.R. Lee, D.S. Alonzi, J. Rountree, S.F. Jenkinson, G.W.J. Fleet, R.A. Dwek, J.H. Jones, T.D. Butters, Synthesis and biological characterisation of novel N-alkyl-deoxynojirimycin α-glucosidase inhibitors, Chem. Biol. Chem. 10 (2009) 1101–1105.
[10] P.S. Sunkara, M.S. Kang, T.L. Bowlin, P.S. Liu, A.S. Tyms, A. Sjoerdsma, Inhibition of glycoprotein processing and HIV replication by castanospermine analogues, Ann. N. Y. Acad. Sci. 616 (1990) 90–96.
[11] L.J. Scott, C.M. Spencer, Miglitol, Drugs 59 (2000) 521–549.
[12] T. Matsuo, H. Odaka, H. Ikeda, Effect of an intestinal disaccharidase inhibitor (AO-128) on obesity and diabetes, Am. J. Clin. Nutr. 55 (1992) 314S–317S.
[13] D. Schmidt, W. Frommer, B. Junge, L. Muller, W. Wingender, E. Truscheit, D. Schäfer, α-Glucosidase inhibitors, Naturwissenschaften 64 (1977) 535–536.
[14] N. Asano, K. Oseki, E. Tomioka, H. Kizu, K. Matsui, *N*-containing sugars from Morus alba and their glycosidase inhibitory activities, Carbohydr. Res. 259 (1994) 243–255.
[15] P. Hollander, Safety profile of acarbose, an α-glucosidase inhibitor, Drugs 44 (1992) 47–53.
[16] A.J. Scheen, Is there a role for α-glucosidase inhibitors in the prevention of type 2 diabetes mellitus, Drugs 63 (2003) 933–951.
[17] A.J. Reuser, H.A. Wisselaar, An evaluation of the potential side-effects of α-glucosidase inhibitors used for the management of diabetes mellitus, Eur. J. Clin. Investig. 24 (1994) 19–24.
[18] S. Sou, S. Mayumi, H. Takahashi, R. Yamasaki, S. Kadoya, M. Sodeoka, Y. Hashimoto, Novel α-glucosidase inhibitors with a tetrachlorophthalimide skeleton, Bioorg. Med. Chem. Lett. 10 (2000) 1081–1084.
[19] S. Adisakwattana, K. Sookkongwaree, S. Roengsumran, A. Petsom, N. Ngamrojnavanich, W. Chavasiri, S. Deesamer, S. Yibchok-anun, Structure–activity relationships of trans-cinnamic acid derivatives on α-glucosidase inhibition, Bioorg. Med. Chem. Lett. 14 (2004) 2893–2896.
[20] W. Puls, U. Keup, H.P. Krause, G. Thomas, F. Hoffiester, Glucosidase inhibition, Naturwissenschaften 64 (1977) 536–537.
[21] Y.J. Shim, H.K. Doo, S.Y. Ahn, Y.S. Kim, J.K. Seong, I.S. Park, B.H. Kim, Inhibitory effect of aqueous extract from the gall of Rhus chinensis on alpha-glucosidase activity and postprandial blood glucose, J. Ethnopharmacol. 85 (2003) 283–287.
[22] W. Benalla, S. Bellahcen, M. Bnouham, Antidiabetic medicinal plants as a source of alpha glucosidase inhibitors, Curr. Diabetes Rev. 6 (2010) 247–254.
[23] E.B. De Melo, A. da Silveira Gomes, I. Carvalho, α-and β-Glucosidase inhibitors: chemical structure and biological activity, Tetrahedron 62 (2006) 10277–10302.
[24] J.W. Dennis, S.L.C. Waghorne, M.L. Breitman, R.S. Kerbel, Beta 1-6 branching of Asn-linked oligosaccharides is directly associated with metastasis, Science 236 (1987) 582–585.
[25] C. Durinx, A.M. Lambeir, E. Bosmans, J.B. Falmagne, R. Berghmans, A. Haemers, S. Scharpé, I. De Meester, Molecular characterization of dipeptidyl peptidase activity in serum: soluble CD26/dipeptidyl peptidase IV is responsible for the release of X-Pro dipeptides, Eur. J. Biochem. 267 (2000) 5608–5613.
[26] D. Lee, J.K. Woo, D. Kim, M. Kim, S.K. Cho, J.H. Kim, S.P. Park, H.Y. Lee, K.Z. Riu, D.-S. Lee, Antiviral activity of methylelaiophylin, an α-glucosidase inhibitor, J. Microbiol. Biotechnol. 21 (2011) 263–266.
[27] G.S. Jacob, Glycosylation inhibitors in biology and medicine, Curr. Opin. Struct. Biol. 5 (1995) 605–611.
[28] E. Simsek, X. Lu, S. Ouzounov, T.M. Block, A.S. Mehta, alpha-Glucosidase inhibitors have a prolonged antiviral effect against hepatitis B virus through the sustained inhibition of the large and middle envelope glycoproteins, Antivir. Chem. Chemother. 17 (2006) 259–267.
[29] M. Singh, M. Kaur, O. Silakari, Flavones: an important scaffold for medicinal chemistry, Eur. J. Med. Chem. 84 (2014) 206–239.
[30] J.D. Xu, L.W. Zhang, Y.F. Liu, Synthesis and antioxidant activities of flavonoids derivatives, troxerutin and 3′,4′,7-triacetoxyethoxyquercetin Chin, Chem. Lett. 24 (2013) 223–226.
[31] J.B. Zheng, H.F. Zhang, H. Gao, Investigation on electrochemical behavior and scavenging superoxide anion ability of chrysin at mercury electrode topon, J. Chem. 23 (2005) 1042–1046.
[32] H.D. Ly, S.G. Withers, Mutagenesis of glycosidases, Annu. Rev. Biochem. 68 (1999) 487–522.
[33] T. Schewe, Y. Steffen, H. Sies, How do dietary flavanols improve vascular function? A position paper, Arch. Biochem. Biophys. 476 (2008) 102–106.
[34] M.N. Clifford, Chlorogenic acids and other cinnamates – nature, occurrence and dietary burden, J. Sci. Food Agric. 79 (1999) 362–372.
[35] M. Richelle, I. Tavazzi, E. Offord, Comparison of the antioxidant activity of commonly consumed polyphenolic beverages (coffee, cocoa, and tea) prepared per cup serving, J. Agric. Food Chem. 49 (2001) 3438–3442.
[36] A. Crozier, I.B. Jaganath, M.N. Clifford, Dietary phenolics: chemistry, bioavailability and effects on health, Nat. Prod. Rep. 26 (2009) 1001–1043.
[37] Q.Q. Wang, N. Cheng, X.W. Zheng, S.M. Peng, X.Q. Zou, Synthesis of organic nitrates of luteolin as a novel class of potent aldose reductase inhibitors, Bioorg. Med. Chem. 21 (2013) 4301–4310.
[38] J.H. Cui, D. Hu, X. Zhang, Z. Jing, J. Ding, R.-B. Wang, S.-S. Li, Design and synthesis of new 7, 8-dimethoxy-a-naphthoflavones as CYP1A1 inhibitors, Chin. Chem. Lett. 24 (2013) 215–218.
[39] K. Hanhineva, R. Törrönen, I. Bondia-Pons, J. Pekkinen, M. Kolehmainen, H. Mykkänen, K. Poutanen, Impact of dietary polyphenols on carbohydrate metabolism, Int. J. Mol. Sci. 11 (2010) 1365–1402.
[40] T. Nishioka, J. Kawabata, Y. Aoyama, Baicalein, an α-glucosidase inhibitor from Scutellaria baicalensis, J. Nat. Prod. 61 (1998) 1413–1415.
[41] H.W. Ryu, B.W. Lee, M.J. Curtis-Long, S. Jung, Y.B. Ryu, W.S. Lee, K.H. Park, Polyphenols from Broussonetia papyrifera displaying potent α-glucosidase inhibition, J. Agric. Food Chem. 58 (2009) 202–208.
[42] M. Taha, N.H. Ismail, M. Ali, K.M. Khan, W. Jamil, S.M. Kashif, M. Asraf, Synthesis of Indole-2-hydrazones in search of potential leishmanicidal agents, Med. Chem. Res. 23 (2014) 5282–5293.
[43] A.N. Aziz, M. Taha, N.H. Ismail, E.H. Anouar, S. Yousuf, W. Jamil, K. Awang, N. Ahmat, K.M. Khan, S.M. Kashif, Synthesis, crystal structure, DFT studies and evaluation of the antioxidant activity of 3,4-dimethoxybenzenamine schiff bases, Molecules 19 (2014) 8414–8433.
[44] a) K.M. Khan, M. Irfan, M. Ashraf, M. Taha, S.M. Saad, S. Perveen, M.I. Choudhary, Synthesis of phenyl thiazole hydrazones and their activity against glycation of proteins, Med. Chem. Res. 24 (2015) 3077–3085;
b) K.M. Khan, M. Taha, F. Rahim, M.I. Fakhri, S. Rasheed, W. Jamil, M. Khan, A. Karim, S. Perveen, M.I. Choudhary, Acylhydrazide schiff bases: synthesis and antiglycation activity, J. Chem. Soc. Pak. 35 (2013) 930–938;
c) K.M. Khan, F. Rahim, N. Ambreen, M. Taha, M. Khan, H. Jahan, A. Shaikh, S. Iqbal, S. Perveen, M.I. Choudhary, Synthesis of benzophenonehydrazone Schiff bases and their in vitro antiglycating activities, Med. Chem. 9 (2013) 588–595.
[45] S. Imran, M. Taha, N.H. Ismail, K.M. Khan, F. Naz, M. Hussain, S. Tauseef, Synthesis of novel bisindolylmethane schiff bases and their antibacterial activity, Molecules 19 (2014) 11722–11740.
[46] M. Taha, N.H. Ismail, S. Imran, M.Q. Rokei, S.M. Saad, K.M. Khan, Synthesis of new oxadiazole derivatives as α-glucosidase inhibitors, Bioorg. Med. Chem. 23 (2015) 4155–4162.
[47] a) M. Taha, N.H. Ismail, W. Jamil, H. Rashwan, S.M. Kashif, A.A. Sain, M.I. Adenan, E.H. Anouar, M. Ali, F. Rahim, K.M. Khan, Synthesis of novel derivatives of 4-methylbenzimidazole and evaluation of their biological activities, Eur. J. Med. Chem. 84 (2014) 731–738;
b) Z.S. Saify, A. Kamil, S. Akhtar, M. Taha, A. Khan, K.M. Khan, S. Jahan, F. Rahim, S. Perveen, M.I. Choudhary, 2-(2′-Pyridyl) benzimidazole derivatives and their urease inhibitory activity, Med. Chem. Res. 23 (2014) 4447–4454;
c) M. Taha, N.H. Ismail, S. Lalani, M.Q. Fatmi, Atia-tul-Wahab, S. Siddiqui, K.M. Khan, S. Imran, M.I. Choudhary, Synthesis of novel inhibitors of α-glucosidase based on the benzothiazole skeleton containing benzohydrazide moiety and their molecular docking studies, Eur. J. Med. Chem. 92 (2015) 387–400;
d) M. Taha, N.H. Ismail, M.S. Baharudin, S. Lalani, S. Mehboob, K.M. Khan, S. yousuf, S. Siddiqui, F. Rahim, M.I. Choudhary, Med. Chem. Res. 24 (2015) 1310;
e) K.M. Khan, F. Rahim, A. Wadood, N. Kosar, M. Taha, S. Lalani, A. Khan, M.I. Fakhri, M. Junaid, W. Rehman, M. Khan, S. Perveen, M. Sajid, M.I. Choudhary, Synthesis and molecular docking studies of potent α-glucosidase inhibitors based on biscoumarin skeleton, Eur. J. Med. Chem. 81 (2014) 245–252.
[48] M. Yar, M. Bajda, L. Shahzadi, S.A. Shahzad, M. Ahmed, M. Ashraf, U. Alam, I.U. Khan, A.F. Khan, Novel synthesis of dihydropyrimidines for a-glucosidase inhibition to treat type 2 diabetes: in vitro biological evaluation and in silico docking, Bioorg. Chem. 54 (2014) 96–104.
[49] a) M. Taha, N.H. Ismail, M.S. Baharudin, S. Lalani, S. Mehboob, K.M. Khan, S. Yousuf, S. Siddiqui, F. Rahim, M.I. Choudhary, Synthesis crystal structure of 2-methoxybenzoylhydrazones and evaluation of their a-glucosidase and urease inhibition potential, Med. Chem. Res. 24 (2015) 1310–1324;
b) M. Taha, H. Naz, S. Rasheed, N.H. Ismail, A.A. Rahman, S. Yousuf, M.I. Choudhary, Synthesis of 4-methoxybenzoylhydrazones and evaluation of their antiglycation activity, Molecules 19 (2014) 1286–1301;
c) F. Rahim, K. Ullah, H. Ullah, A. Wadood, M. Taha, A.U. Rehman, U. Imad, A. Muhammad, S. Ayesha, R. Wajid, H. Shafqat, K.M. Khan, Triazinoindole analogs as potent inhibitors of α-glucosidase: synthesis, biological evaluation and molecular docking studies, Bioorg. Chem. 58 (2015) 81–87.
[50] X. Li, E.S. Inks, X. Li, J. Hou, C.J. Chou, J. Zhang, J. Yuqi, Z. Yingjie, W. Xu,

Discovery of the first N-hydroxycinnamamide-based histone deacetylase 1/3 dual inhibitors with potent oral antitumor activity, J. Med. Chem. 57 (2014) 3324–3341.
[51] E. Borenfreund, H. Babich, N. Martin-Alguacil, Comparisons of two in vitro cytotoxicity assays - the neutral red (NR) and tetrazolium MTT tests, Toxic. In Vitro 2 (1988) 1–6.
[52] G.M. Morris, R. Huey, W. Lindstrom, M.F. Sanner, R.K. Belew, D.S. Goodsell, A.J. Olson, Autodock4 and AutoDockTools4: automated docking with selective receptor flexibility, J. Comput. Chem. 16 (2009) 2785–2791.
[53] F. Kiefer, K. Arnold, M. Kunzli, L. Bordoli, T. Schwede, The SWISS-MODEL repository and associated resources, Nucleic Acids Res. 37 (2009) D387–D392.
[54] K. Arnold, L. Bordoli, J. Kopp, T. Schwede, The SWISS-MODEL workspace: a web-based environment for protein structure homology modelling, Bioinformatics 22 (2006) 195–201.
[55] N. Guex, M.C. Peitsch, T. Schwede, Automated comparative protein structure modelling with swiss-model and Swiss-Pdb viewer: a historical perspective, Electrophoresis 30 (2009) S162–S173.
[56] Accelrys Software Inc., Discovery Studio Modeling Environment, Release 3.5, Accelrys Software Inc, San Diego, 2012.
[57] The PyMol Molecular Graphics System, Version 1.1 Schrödinger, LLC.
[58] A.L. Morris, M.W. MacArthur, E.G. Hutchinson, J.M. Thornton, Stereochemical quality of protein structure coordinates, Proteins Struct. Funct. Bioinform. 12 (1992) 345–364.
[59] R.A. Laskowski, J.A. Rullmannn, M.W. MacArthur, R. Kaptein, J.M. Thornton, AQUA and PROCHECK-NMR: programs for checking the quality of protein structures solved by NMR, J. Biomol. NMR 8 (1996) 477–486.